Interplay of Structure and Diffusion in Ternary Liquid Mixtures of Benzene + Acetone + Varying Alcohols[a)]

Gabriela Guevara-Carrion,[1] Yuri Gaponenko,[2] Aliaksandr Mialdun,[2] Tatjana Janzen,[1] Valentina Shevtsova,[2, b)] and Jadran Vrabec[1, c)]

[1)] *Thermodynamics and Energy Technology, University of Paderborn, Warburger Str. 100, D-33098 Paderborn, Germany*

[2)] *Microgravity Research Center, Université Libre de Bruxelles, CP–165/62, Av. F.D. Roosevelt, 50, B–1050 Brussels, Belgium*

(Dated: 11 August 2018)

The Fick diffusion coefficient matrix of ternary mixtures containing benzene + acetone + three different alcohols, i.e. methanol, ethanol and 2-propanol, is studied by molecular dynamics simulation and Taylor dispersion experiments. Aiming to identify common features of these mixtures, it is found that one of the main diffusion coefficients and the smaller eigenvalue do not depend on the type of alcohol along the studied composition path. Two mechanisms that are responsible for this invariant behavior are discussed in detail, i.e. the interplay between kinetic and thermodynamic contributions to Fick diffusion coefficients and the presence of microscopic heterogeneities caused by hydrogen bonding. Experimental work alone cannot explain these mechanisms, while present simulations on the molecular level indicate structural changes and uniform intermolecular interactions between benzene and acetone molecules in the three ternary mixtures. The main diffusion coefficients of these ternary mixtures exhibit similarities with their binary subsystems. Analyses of radial distribution functions and hydrogen bonding statistics quantitatively evidence alcohol self-association and cluster formation, as well as component segregation. Further, the excess volume of the mixtures is analyzed in the light of intermolecular interactions, further demonstrating the benefits of the simultaneous use of experiment and simulation. The proposed framework for studying diffusion coefficients of a set of ternary mixtures, where only one component varies, opens the way for further investigations and a better understanding of multicomponent diffusion. The presented numerical results may also give an impulse to the development of predictive approaches for multi-component diffusion.

Keywords: ternary diffusion, Taylor dispersion, transport properties, microscopic structure, hydrogen bonding, molecular simulation

---

[a)]Supplementary Materials available.

[b)]Electronic mail: vshev@ulb.ac.be

[c)]Electronic mail: jadran.vrabec@upb.de

I. INTRODUCTION

In recent years, molecular modelling and simulation has been established as a reliable tool to study transport properties of liquids because it allows to uncover the involved physical mechanisms at the molecular level. Consequently, academic work that combines experiments and molecular simulation has gained popularity[1–5]. Such joint investigations do not only offer the possibility to contrast experimental results, but also to consider microscopic details which, in many cases, are inaccessible with experimental techniques[6].

Most mass transfer processes occurring in natural phenomena and engineering applications involve multicomponent liquid solutions that are thus of great importance for basic and applied research[7]. However, diffusion coefficients have experimentally been measured only for a very limited number of mixtures containing three or more components. In fact, the description of multicomponent diffusion is more challenging than it is often conceived. For instance, a ternary mixture has four state dependent Fick diffusion coefficients which differ with component order and reference frame. The presence of cross diffusion effects introduces additional complexity into experimental data interpretation and processing[8,9]. Indeed, the first experimental verification of the existence of cross diffusion was reported a century after[10] the first experimental and theoretical investigations of binary liquid mixtures[11]. Hence, there is significant interest in the improvement of experimental methodologies and the development of reliable methods for the prediction of mutual diffusion coefficients of liquid mixtures containing three or more components.

Experimental and molecular simulation techniques were employed in this work to obtain diffusion coefficients and density of three ternary liquid mixtures constituted of an aromatic, a ketone and an alcohol. Benzene and acetone were mixed with one of the following three alcohols: methanol, ethanol or 2-propanol. For each mixture, nine state points along a composition path with a constant benzene mole fraction of $x_1 = 0.33$ mol mol^{-1} were studied under ambient conditions of temperature and pressure. These ternary mixtures contain non-polar, polar aprotic and protic associating components that also significantly differ in molecular mass and size. These characteristics make them particularly challenging[12], but also interesting as model mixtures to study the influence of the alcohol carbon chain length on diffusion phenomena. Selected pioneering results on these mixtures were recently published[13], showing an intriguing relationship between the kinetic and thermodynamic

contributions to the Fick diffusion coefficients. Thus, the aim of this study was not only to determine the Fick diffusion coefficient matrix, but also to seek for common features that may help to better understand complex diffusion processes and support the development and verification of predictive approaches.

In their pure liquid state, alcohol molecules exist in a self-associated form, while benzene and acetone molecules exhibit non-associated structures[14]. Thus, when an alcohol is mixed with benzene and acetone, different intermolecular interactions will lead to an extensive variation of molecular ordering, which entails interesting macroscopic properties. Therefore, to understand the observed dynamic behavior from a microscopic point of view on the basis of structural properties, radial distribution functions (RDF) and hydrogen bonding statistics were also analyzed.

Experimentally, Fick diffusion coefficients can be measured with a variety of techniques from optical interferometry to NMR spin relaxation. In the present work, Taylor dispersion, also known as peak broadening technique, was employed. On the molecular simulation side, transport properties were sampled with equilibrium molecular dynamics and the Green-Kubo formalism.

To the best of our knowledge, only one of the regarded ternary mixtures, i.e. benzene + acetone + methanol, has been studied with respect to diffusion before[15]. Diffusion and structural properties of several binary subsystems that involve methanol or ethanol have been the subject of investigations[16–23]. Binary mixtures of acetone with methanol[5,14,24,25] or ethanol[26] have been studied especially with respect to their ability to form hydrogen bonds. Attention has also been paid to the structural properties of binary mixtures of benzene with methanol, ethanol or acetone[27–31].

Molecular simulation studies on diffusion coefficients of ternary liquid mixtures containing associating species are still scarce. Preceding work of our group on water + methanol + ethanol[3,32], the work of Liu et al.[33,34] on chloroform + acetone + methanol and water + methanol + ethanol as well as the investigation of transport properties of acetone + water + supercritical CO_2 by Sohrevardi et al.[35] should be mentioned. The present study continues our efforts to combine molecular simulation and experimental work to analyze diffusion in ternary liquid mixtures.

This paper is organized as follows: First, a brief explanation of the general equations governing diffusive fluxes in ternary mixtures is given. Second, the experimental methodology is

described, followed by a brief outline of the employed simulation techniques. Subsequently, the experimental and simulation results are presented and analyzed in the light of the observed microscopic structure. For this purpose, hydrogen bonding statistics and RDF were employed. Finally, conclusions are drawn.

II. THEORY OF DIFFUSION

There are two major formulations to describe diffusive mass transport in mixtures. These are Maxwell-Stefan (MS) theory and the generalization of Fick's law, in which the molar flux of component i in a mixture of N components is written as a linear combination of concentration gradients ∇C_j[36]

$$J_i = -\sum_{j=1}^{N-1} D_{ij} \nabla C_j \,, \quad (i = 1, 2, ..., N-1) \,, \tag{1}$$

where D_{ii} are the main diffusion coefficients that relate the molar flux of component i to its own concentration gradient and D_{ij} are the cross diffusion coefficients that relate the molar flux of component i to the concentration gradient of component j[37]. Because molar fluxes, concentration gradients and diffusion coefficients D_{ij} can be determined experimentally, Fick's law is the most widely used approach. However, it suffers from serious drawbacks[38]. The Fick approach involves $N-1$ independent diffusion fluxes and a $(N-1) \times (N-1)$ matrix of diffusion coefficients, which is generally not symmetric, i.e. $D_{ij} \neq D_{ji}$. Further, the numerical values of D_{ij} depend both on the reference frame for velocity (molar-, mass- or volume-averaged) and on the order of the components. In this work, the following the component order was specified: benzene (1) + acetone (2) + methanol / ethanol / 2-propanol (3).

The molar-averaged reference frame was used in the present simulations to obtain Fick diffusion coefficients, where the following closure holds

$$\sum_{i=1}^{N} J_i^M = 0 \,, \tag{2}$$

for the molar diffusion flux of component i in that reference frame J_i^M. On the other hand, the mathematical model of the Taylor dispersion technique for ternary mixtures was originally developed for the volume-averaged reference frame[39]. In this case, the closure reads

$$\sum_{i=1}^{N} J_i^V v_i = 0\,, \tag{3}$$

where J_i^V is the molar diffusion flux of component i in the volume-averaged reference frame and v_i the partial molar volume of component i. Because the molar fluxes depend on the reference frame choice, the diffusion coefficients are defined accordingly. The Fick diffusion coefficients in the volume- and molar-averaged reference frames are denoted by D_{ij}^V and D_{ij}^M, respectively. The diffusion coefficient matrix in the volume-averaged reference frame $\boldsymbol{D}^V$ is related to the one in the molar-averaged reference frame $\boldsymbol{D}^M$ by[40]

$$\boldsymbol{D}^V = \boldsymbol{B}^{Vu} \cdot \boldsymbol{D}^M \cdot \boldsymbol{B}^{uV}, \tag{4}$$

where

$$\begin{aligned} B_{ij}^{Vu} &= \delta_{ij} - x_i \left(v_j - v_N\right)/v, \\ B_{ij}^{uV} &= \delta_{ij} - x_i \left(1 - v_j/v_N\right), \end{aligned} \tag{5}$$

with δ_{ij} being the Kronecker delta function, x_i the mole fraction of component i and

$$v = \sum_{i=1}^{N} x_i v_i. \tag{6}$$

The main shortcoming of Fick's law is the fact that concentration gradients are not the true thermodynamic driving forces for diffusion, which are rather constituted by chemical potential gradients[41]. MS theory follows this path, assuming that chemical potential gradients $\nabla\mu_i$ are balanced by friction forces between the components that are proportional to their mutual velocity $\boldsymbol{u}_i - \boldsymbol{u}_j$ [40]

$$\sum_{j\neq i=1}^{N} \frac{x_j(\boldsymbol{u}_i - \boldsymbol{u}_j)}{Đ_{ij}} = -\frac{1}{k_\mathrm{B}T}\nabla\mu_i\,, \tag{7}$$

where k_B is the Boltzmann constant and T the temperature. The MS diffusion coefficient $Đ_{ij}$ thus plays the role of an inverse friction coefficient between components i and j. MS diffusion coefficients are symmetric, i.e. $Đ_{ij} = Đ_{ji}$, so that the according matrix has only $N(N-1)/2$ independent entries. Furthermore, these $Đ_{ji}$ pairs do not depend on the component order[42].

Because Fick's law and MS theory describe the same physical phenomenon, the Fick diffusion coefficients can be expressed as

$$\boldsymbol{D}^M = \boldsymbol{\Delta} \cdot \boldsymbol{\Gamma}\,, \tag{8}$$

in which all three symbols represent $(N-1) \times (N-1)$ matrices and $\boldsymbol{\Delta}$ is the matrix of phenomenological diffusion coefficients. In this way, MS diffusion coefficients can be transformed to the Fick diffusion coefficients and vice versa, if the thermodynamic factor matrix $\boldsymbol{\Gamma}$ [40]

$$\Gamma_{ij} = \delta_{ij} + x_i \frac{\partial \ln \gamma_i}{\partial x_j}\bigg|_{T,p,x_{k,k\neq j=1\ldots N-1}}\,. \tag{9}$$

is known. Therein, γ_i stands for the activity coefficient of component i. Further, MS diffusion coefficients are related to the inverse of the phenomenological diffusion coefficient matrix $\boldsymbol{B} = \boldsymbol{\Delta}^{-1}$ by[43]

$$B_{ii} = \frac{x_i}{Đ_{iN}} + \sum_{j\neq i=1}^{N} \frac{x_j}{Đ_{ij}}\,, \qquad B_{ij} = -x_i \left(\frac{1}{Đ_{ij}} - \frac{1}{Đ_{iN}}\right)\,.$$

In Eq. (8), the phenomenological diffusion coefficient matrix $\boldsymbol{\Delta}$ accounts for hydrodynamics, while the thermodynamic factor matrix $\boldsymbol{\Gamma}$ accounts for thermodynamic aspects of diffusion. Clearly, non-ideal solution thermodynamics has a strong influence on diffusion in liquid mixtures[42]. However, it should be noted that these parameters are not completely independent. Intermolecular interactions are at the root because they determine the activity coefficients as well as the effective diffusion ratio governing hydrodynamics[37].

III. TAYLOR DISPERSION EXPERIMENTS

A. Working Equations

The Taylor dispersion technique was used for measurements of the Fick diffusion coefficient matrix. A detailed description of the employed experimental set-up can be found in Refs.[3,8,9] so that only specific information is provided here. As an injected concentration pulse in a carrier liquid is pumped through a long tube, it broadens by the coupled action of convection in axial direction and diffusion in radial direction. The inner diameter and length of the employed polytetrafluoroethylene tube were $2R_0 = 748 \pm 1\,\mu$m and $L = 29.839 \pm 0.001\,$m, respectively. That capillary was coiled around a grooved aluminum

cylinder with a diameter of 30 cm and was placed together with a refractometer and a pump in a temperature-regulated air bath at 298 ± 0.2 K. The flow rate was 0.08 mL / min and the injected volume was 20 μL.

At the end of the capillary, a differential refractometer monitored the composition of the eluted Taylor peak as a function of time t. Its output voltage signal consisted of two overlapping profiles $V_i(t)$

$$V(t) = \sum_{k=0}^{K} V_k t^k + V_1(t) + V_2(t). \tag{10}$$

Fick diffusion coefficients were calculated by comparing the experimental refractive index profile with the analytical solution. For a practical implementation following Leaist[44], the solution of the system of two diffusion equations was transformed to describe the detector output signal $V(t)$

$$\begin{aligned} V(t) = &\sum_{k=0}^{K} V_k t^k + \Delta V_{\max} \sqrt{\frac{t_R}{t}} \\ &\times \left[W_1 \exp(-\hat{D}_1 \eta) + (1 - W_1) \exp(-\hat{D}_2 \eta) \right], \end{aligned} \tag{11}$$

where $\eta = 12(t - t_R)^2 / R_0^2 t$, $t_R = L/u$ is the retention time, $\Delta V_{\max}$ is the maximal peak height at $t = t_R$ and $\hat{D}_i$ are the eigenvalues of the Fick diffusion coefficient matrix

$$\hat{D}_{1,2} = \frac{1}{2} \left(D_{11}^V + D_{22}^V \pm \sqrt{(D_{11}^V - D_{22}^V)^2 + 4 D_{12}^V D_{21}^V} \right). \tag{12}$$

The normalized weight W_1 is defined as

$$W_1 = \frac{(a + b\alpha)\sqrt{\hat{D}_2}}{(a + b\alpha)\sqrt{\hat{D}_1} + (1 - a - b\alpha)\sqrt{\hat{D}_2}}, \tag{13}$$

where the parameters are

$$a = \frac{D_{11}^V - \hat{D}_1 - D_{12}^V S_R}{\hat{D}_2 - \hat{D}_1}, \tag{14}$$

$$b = \frac{D_{22}^V - D_{11}^V - D_{21}^V / S_R + D_{12}^V S_R}{\hat{D}_2 - \hat{D}_1}, \tag{15}$$

$$\alpha = \frac{\Delta C_1}{\Delta C_1 + \Delta C_2 / S_R}. \tag{16}$$

An unconstrained Nelder-Mead simplex method, similar to that employed by Legros et al.[9], was used to fit the working equations to the experimental voltage data from the refractive index detector. Instead of a direct fit of the Fick diffusion coefficients D_{ij}^V, the coefficients a, b and the two eigenvalues $\hat{D}_i$ were adjusted[45]. As can be seen from Eqs. (13-16), the experimental signal strongly depends on the parameter S_R, which is a sensitivity ratio of the detector with respect to the independent components. Basic tests and validations of the experimental set-up with binary and ternary mixtures were presented in detail in Refs.[3,8,9]. Instead, attention will be drawn to the determination of the optical sensitivity coefficient S_R for the considered mixtures which contributes substantially to the accuracy of Taylor measurements when applied to ternary mixtures.

B. Optical Properties

Refractometers provide an electrical signal, which depends on a change of the refractive index n. Their voltage output signal $V(t)$ is assumed to be linearly proportional to small concentration changes of all independent components of the mixture[44]

$$V(t) = \sum_{k=0}^{K} V_k t^k + R_1(C_1(t) - C_1^0) + [R_2(C_2(t) - C_2^0)]. \tag{17}$$

Therein, C_i^0 and C_i are the molar concentrations of the liquid carrier mixture and injection, respectively. The first term in Eq. (17) describes the baseline drift of the detector and was modeled by a second order polynomial, $K = 2$. The sensitivity of the refractometer on component i in the mixture can be written as

$$R_i = \partial V/\partial C_i = (\partial V/\partial n)(\partial n/\partial C_i),$$

where $(\partial V/\partial n)$ is detector constant and the derivatives $\partial n/\partial C_i$ are the contrast factors. Note that the sensitivity ratio S_R in Eqs. (11-16) does not depend on the detector constant

$$S_R = R_1/R_2 = (\partial n/\partial C_1)/(\partial n/\partial C_2).$$

Optical contrast factors can be determined by independent measurements of the refractive index. Alternatively, the sensitivity ratio S_R can be determined from the ratio of the surface areas between the dispersion peak and the baseline for different injections. However, initial

experimental runs did not allow for a reliably determination of S_R by the second approach, which motivated the dedicated measurement of the refractive index.

In experimental work, it is preferred to deal with directly accessible composition variables like mole fractions x_i. On that basis, the optical contrast can be written as

$$\frac{\partial n}{\partial C_i} = \frac{\partial n}{\partial x_i}\frac{\partial x_i}{\partial C_i}, \tag{18}$$

with

$$\frac{\partial x_i}{\partial C_i} = v\left[1 - x_i\left(1 - \frac{v_i}{v_3}\right)\right]. \tag{19}$$

To determine optical contrast factors, 27 solutions with varying composition were prepared for each ternary mixture, i.e., nine state points along three paths with a constant benzene mole fraction $x_1 = 0.26$, 0.33 and 0.40 mol mol^{-1}, cf. Fig. 1 (top). For this purpose, the following substances were purchased and used without further purification: benzene (CAS number 71-43-2) from Sigma-Aldrich, acetone (CAS number 67-64-1) from Merck, methanol (CAS number 65-56-1) from Fisher, ethanol (CAS number 64-17-5) from VWR and 2-propanol (CAS number 67-63-0) from Sigma-Aldrich.

The differential refractometer operated at $\lambda = 950$ nm and the measurements were carried out at the nearest accessible wavelength $\lambda = 935$ nm, cf. Fig. 1. In case of the ternary mixture containing methanol, the refractive index $n(x_1, x_2)$ has a very weak composition dependence and was thus additionally measured at wavelengths of $\lambda = 590$ and 670 nm, considering the dispersion dependence given by the Cauchy equation[46]

$$n(\lambda) = A + \frac{B}{\lambda^2}.$$

Constants A and B were determined by comparing measurements at different wavelengths.

The dependence of the refractive index on the acetone mole fraction x_2 was approximated by third order polynomials. Although their relation was nearly linear in some cases, the third order was kept throughout for the sake of consistency

$$n(x_2) = a_3 \cdot x_2^3 + a_2 \cdot x_2^2 + a_1 \cdot x_2 + a_0, \tag{20}$$

for a given benzene mole fraction x_1. The coefficients for all mixtures are listed in Table II. The derivative $(\partial n/\partial x_2)_{x_1}$ can be determined from Eq. (20) by differentiation. The other

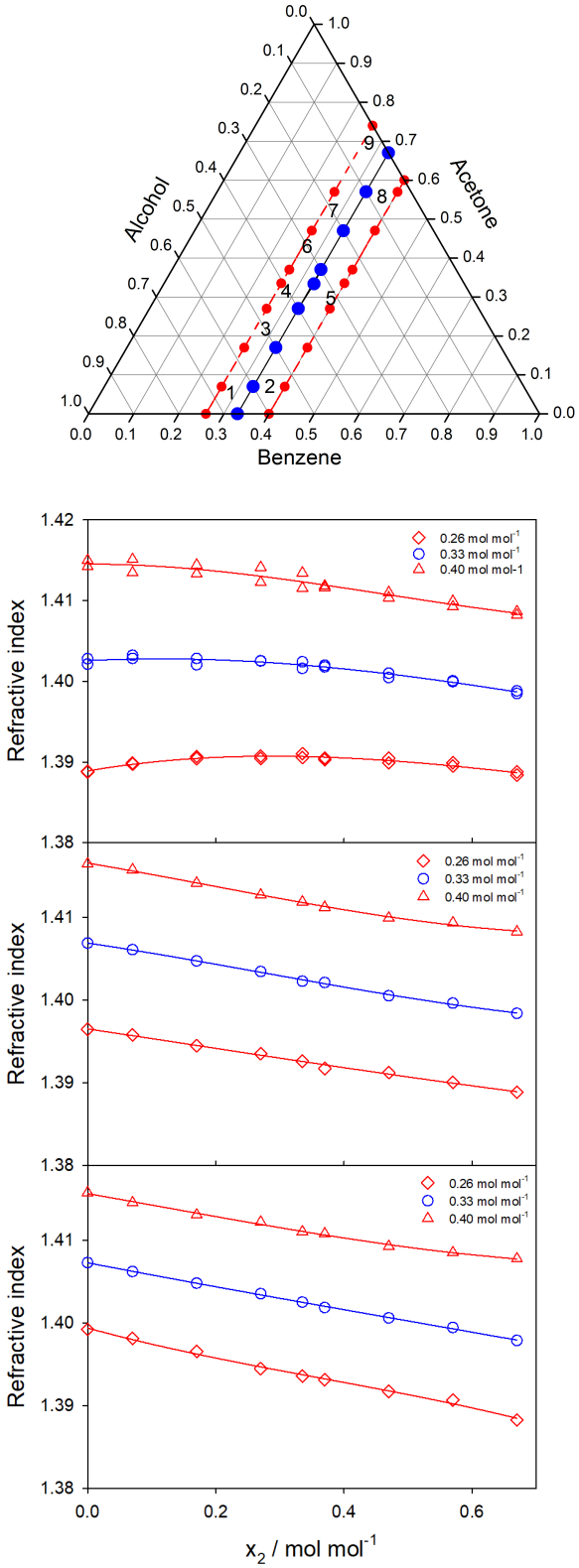

FIG. 1. Refractive index n of the ternary mixtures benzene + acetone + methanol (top) / ethanol (center) / 2-propanol (bottom) at 298.15 K, 0.1 MPa and $\lambda = 935$ nm along three constant benzene mole fraction paths $x_1 = 0.26$, 0.33 and 0.40 mol mol^{-1}. x_2 stands for the acetone mole fraction.

TABLE I. Coefficients of Eq. (20) for the refractive index of the ternary mixtures benzene + acetone + methanol / ethanol / 2-propanol at 298.15 K, 0.1 MPa and λ=935 nm along the three constant benzene mole fraction paths $x_1 = 0.26$, 0.33 and 0.40 mol mol^{-1} as shown in Fig. 1.

x_1	a_0	a_1	a_2	a_3
mol mol^{-1}		benzene + acetone + methanol		
0.26	1.4145	0.0003	−0.0270	0.0193
0.33	1.4026	0.0042	−0.0198	0.0073
0.40	1.3889	0.0137	−0.0289	0.0119
		benzene + acetone + ethanol		
0.26	1.4166	−0.0132	−0.0078	0.0137
0.33	1.4069	−0.0115	−0.0086	0.0105
0.40	1.3965	−0.0118	−0.0007	0.0020
		benzene + acetone + 2-propanol		
0.26	1.4156	−0.0137	−0.0024	0.0078
0.33	1.4073	−0.0149	0.0026	0.0016
0.40	1.3994	−0.0212	0.0186	−0.0169

derivative $(\partial n/\partial x_1)_{x_2}$ was calculated on the basis of measurements at three state points with a constant mole fraction x_1, expressed by the linear equation

$$(\partial n/\partial x_1)_{x_2} = d_1 \cdot x_2 + d_0. \tag{21}$$

TABLE II. Coefficients of Eq. (21) for $(\partial n/\partial x_1)_{x_2}$ of benzene + acetone + alcohol mixtures at $\lambda = 935$ nm.

alcohol	d_0	d_1
methanol	0.0280	−0.0251
ethanol	−0.0142	0.0038
2-propanol	−0.0145	0.0019

The contrast factors of all mixtures are shown in Fig. 2. There are two important conclusions: first, $(\partial n/\partial x_1)_{x_2}$ is larger than $(\partial n/\partial x_2)_{x_1}$ by more than one order of magnitude, meaning that the detector signal has little sensitivity on the acetone mole fraction. Second, the value of $(\partial n/\partial x_2)_{x_1}$ is zero at $x_2 = 0.12$ mol mol^{-1} and within the small margins along the

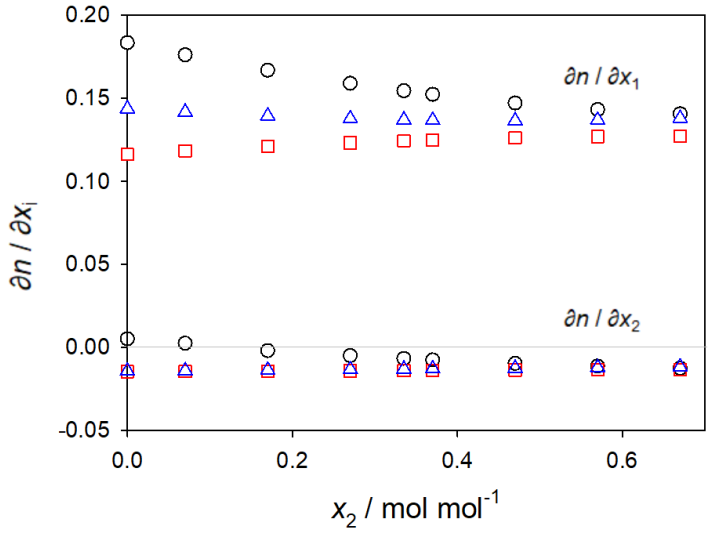

FIG. 2. Optical contrast factors of the ternary mixtures benzene + acetone + methanol (black) / ethanol (blue) / 2-propanol (red) at 298.15 K, 0.1 MPa and $\lambda = 935$ nm along a constant benzene mole fraction path $x_1 = 0.33$ mol mol^{-1}. x_2 stands for the acetone mole fraction.

path $x_1 = 0.33$ mol mol^{-1} it can be positive or negative, which may lead to very different contributions of the last two terms in Eq. (17). This imposes limitations on the selection of the injection composition and requires numerous repetitions of Taylor measurements runs. For example, it was not favorable to take two perpendicular injections in which either $\Delta x_1 = 0$ or $\Delta x_2 = 0$. The choice of the injection composition in regions with poor optical properties was discussed in detail in Ref.[3]. Note that the main Fick diffusion coefficients D_{11}^V and D_{22}^V were much less affected by the choice of the injection composition than the cross diffusion coefficients D_{12}^V and D_{21}^V.

Solutions for the Fick diffusion coefficients obtained by the fitting procedure were stable, however, the cross diffusion coefficients of the diffusion matrix display larger differences from molecular dynamics simulation results. It is important to note that in case of mixtures with methanol, the present simulation results provided valuable support to the experiments as they were used as initial guess.

Optical contrast factors of these mixtures are valuable not only for the study of diffusion, but also for other laboratory work which relies on such data, e.g. Soret experiments[47].

IV. MOLECULAR SIMULATION

Rigid, united-atom type models were used to describe the intermolecular interactions. The employed molecular models account for these interactions, including hydrogen bonding, by a set of Lennard-Jones (LJ) sites, point charges, point dipoles and point quadrupoles, which may or may not coincide with the LJ site positions[48–52]. These models were satisfactorily assessed in previous works with respect to the binary subsystems of the ternary mixtures under consideration[48]. The interested reader is referred to the original publications[48–52] for detailed information about the molecular pure substance models and their parameters.

To define a molecular model for a ternary mixture on the basis of pairwise additive potentials, only the unlike interactions have to be specified. In case of polar interaction sites, this can straightforwardly be done by following the laws of electrostatics. However, for the unlike LJ parameters, there is no physically sound approach so that combining rules have to be employed for predictions. For this purpose, the simple Lorentz-Berthelot combining rules were chosen. Consequently, all simulation data presented below are strictly predictive.

The Green-Kubo formalism based on the net velocity auto-correlation function can be employed to sample the Onsager coefficients[43]

$$\lambda_{ij} = \frac{1}{3N_p} \int_0^\infty \mathrm{d}t \left\langle \sum_{k=1}^{N_{p,i}} \mathrm{v}_{i,k}(0) \cdot \sum_{l=1}^{N_{p,j}} \mathrm{v}_{j,l}(t) \right\rangle , \tag{22}$$

where N_p is the total number of molecules, $N_{p,i}$ is the number of molecules of component i and $\boldsymbol{v}_{i,k}(t)$ denotes the center of mass velocity vector of the k-th molecule of component i at time t. Eq. (22) corresponds to a reference frame in which the mass-averaged mixture velocity is zero[43]. Note that the $\boldsymbol{\lambda}$ matrix is symmetric because of the Onsager reciprocal relations[53]. For a ternary mixture, the elements of the phenomenological diffusion coefficient matrix $\boldsymbol{\Delta}$ in the molar-averaged reference frame are then given by[43]

$$\Delta_{11} = (1-x_1)\left(\frac{\lambda_{11}}{x_1} - \frac{\lambda_{13}}{x_3}\right) - x_1\left(\frac{\lambda_{21}+\lambda_{31}}{x_1} - \frac{\lambda_{23}+\lambda_{33}}{x_3}\right),$$
$$\Delta_{12} = (1-x_1)\left(\frac{\lambda_{12}}{x_2} - \frac{\lambda_{13}}{x_3}\right) - x_1\left(\frac{\lambda_{22}+\lambda_{32}}{x_2} - \frac{\lambda_{23}+\lambda_{33}}{x_3}\right),$$
$$\Delta_{21} = (1-x_2)\left(\frac{\lambda_{21}}{x_1} - \frac{\lambda_{23}}{x_3}\right) - x_2\left(\frac{\lambda_{11}+\lambda_{31}}{x_1} - \frac{\lambda_{13}+\lambda_{33}}{x_3}\right),$$
$$\Delta_{22} = (1-x_2)\left(\frac{\lambda_{22}}{x_2} - \frac{\lambda_{23}}{x_3}\right) - x_2\left(\frac{\Lambda_{12}+\lambda_{32}}{x_2} - \frac{\lambda_{13}+\lambda_{33}}{x_3}\right). \quad (23)$$

The Fick diffusion coefficient matrix was thus determined through Eqs. (8) and (23). Further, once the phenomenological diffusion coefficient matrix $\mathbf{\Delta}$ is known, the MS diffusion coefficients can be calculated from Eq. (10).

A recent work of Jamali et al.[54] demonstrated the presence of a significant system size dependence on the calculated values of the binary MS diffusion coefficients. They suggest that the finite-size effect, which is also found for self- and intra-diffusion coefficients, is highly dependent on the nonideality of the mixture and thus, on the thermodynamic factor. Therefore, it is expected that present ternary simulation results exhibit systematic errors due to finite-size effects. However, because of the relatively large number of molecules (5000) employed, the errors are expected to be within the statistical uncertainties of the simulation results.

The thermodynamic factor matrix $\mathbf{\Gamma}$ was calculated from the classical Wilson[55] excess Gibbs energy G^{E} model, which does yield good results for the present binary subsystems[48]. The Wilson G^{E} model relies on adjustable binary parameters, which were regressed to experimental vapor-liquid equilibrium data for each binary subsystem, assuming that the vapor phase is an ideal gas and that the Poynting correction factor is negligible. The according regressions were carried out with the RecPar tool from the Dortmund Data Bank[56]. The composition derivatives of the multicomponent Wilson model were evaluated analytically as described by Taylor and Kooijman[57], leading to the thermodynamic factor

$$\Gamma_{ij} = \delta_{ij} + x_i(Q_{ij} - Q_{iN}), \quad (24)$$

and

$$Q_{ij} = -\Lambda_{ij}/S_i - \Lambda_{ji}/S_j + \sum_{k=1}^{N} x_k \Lambda_{ki}\Lambda_{kj}/S_k^2, \quad (25)$$

where

$$S_i = \sum_{j=1}^{N} x_j \Lambda_{ij}, \tag{26}$$

and Λ_{ij} are adjustable Wilson parameters. Their numerical values are given in the supplementary material. Note that this multicomponent thermodynamic model also defines the properties of its binary subsystems.

Structural Properties

The RDF $g(r)$ is an important property to characterize the microscopic structure of matter. It represents the local density around a site or position[58]

$$g(r) = \frac{V}{N^2} \left\langle \sum_i \sum_{j \neq i} \delta(\boldsymbol{r} - \boldsymbol{r_{ij}}) \right\rangle, \tag{27}$$

where N is the number of molecules on a volume V with an average number density $\rho = N/V$.

The geometric criterion proposed by Haughney et al.[59] was employed to sample hydrogen bonding statistics for the studied ternary mixtures. Accordingly, two sites were considered to form a hydrogen bond if the distance between the donor and the acceptor sites was smaller than 2.6 Å, the distance between the acceptor sites of the acceptor and donor molecules was smaller than 3.5 Å and the angle between the acceptor–donor axis and the acceptor–acceptor axis was below 30°.

V. RESULTS

A. Density and Excess Volume

The density of the three ternary mixtures was determined experimentally and predicted by means of molecular simulation. Numerical data are given in Table III. The densities of the solution were measured with a vibrating tube density meter (Anton Paar GmbH, model DMA 5000M) with a standard deviation of $1 \cdot 10^{-2}\,\mathrm{kg\ m^{-3}}$ and internal temperature control of 0.01 K. Further, the excess volume of the mixture was derived from the present experimental data in order to discuss mixing effects due to molecular packing. The excess volume is negative for the ternary mixtures involving methanol or ethanol, indicating denser

molecular packing than in the pure liquids and strongly attractive unlike interactions, cf. Fig. 3. These effects are more pronounced for the mixture containing methanol because of its small molecular size and the presence of strong hydrogen bonding. The minimum of the excess volume is located near equimolar composition for both alcohols. On the other hand, the mixture containing 2-propanol shows a positive excess volume, indicating a decrease in the packing density upon mixing, which is a consequence of the bulky shape of 2-propanol molecules that leads to steric hindrance.

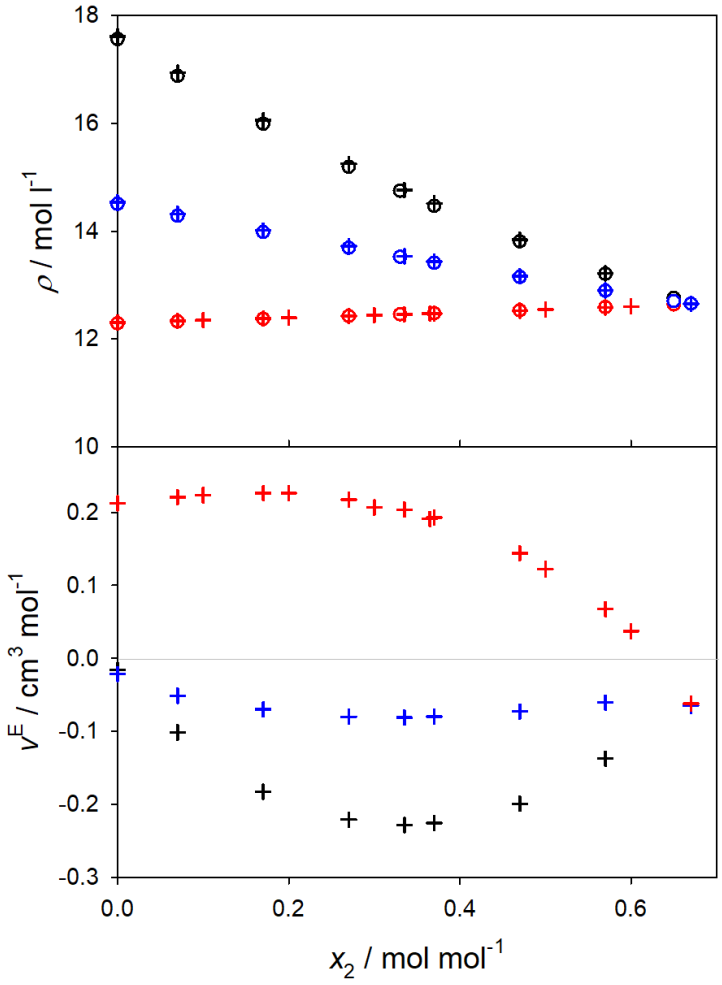

FIG. 3. Density ρ (top) and excess volume v^{E} (bottom) of the mixtures benzene + acetone + methanol (black) / ethanol (blue) / 2-propanol (red) at 298.15 K and 0.1 MPa along a constant benzene mole fraction path $x_1 = 0.33$ mol mol^{-1}. Data from present experiments (+) are compared with present simulation results ($\circ$). x_2 stands for the acetone mole fraction.

B. Intradiffusion Coefficients

Although intradiffusion coefficients bear less practical importance than mutual diffusion coefficients, they provide fundamental information about solvation, structure and dynamics of solutions[60]. The intradiffusion coefficients of all components in the ternary mixtures were thus calculated by molecular simulation and the Green Kubo formalism. Finite size effects were accounted with the correction by Yeh and Hummer[61], which did not exceeded 6% of the simulation results. The results are shown in Fig. 4. The intradiffusion coefficients of both benzene D_1 and acetone D_2 are higher for the ternary mixture involving methanol, which is a consequence of the obstruction effect[60], i.e. their propagation is blocked to a lesser extent through the small and light methanol molecules. For the mixtures involving ethanol or 2-propanol, the intradiffusion coefficients D_1 and D_2 are almost identical. The intradiffusion coefficient of the three alcohols D_3 behaves as expected, mobility decreases with molecular weight. Note that intradiffusion does not always adhere to this rule, e.g. it decreases with the presence of self-association due to hydrogen bonding as is the case for the alcohols. This phenomenon leads to a decrease of mobility of the alcohol molecules, i.e. the increase of their effective diffusion size when the alcohol concentration is increased. In fact, in the alcohol-rich region, the intradiffusion coefficient of the small methanol molecules is similar as that of the much larger benzene molecules.

To understand this phenomenon, the average number of hydrogen bonds per alcohol molecule in the three ternary mixtures was calculated by molecular simulation, cf. Fig. 1 of the supplementary material. In the binary limit $x_2 \to 0$, alcohol molecules are hydrogen bonded on average to ~ 1.8 other alcohol molecules, which approximately coincides with the value for pure alcohols. Along the studied composition path, the average hydrogen bond number decreases to less than unity in the alcohol-poor region. This decrease is almost monotonic up to the equimolar composition where a marked change in the slope can be noticed. This behavior cannot solely be explained by the reduction in the availability of hydrogen bonding partners but also by the disruption of ordered hydrogen bonding structures, which is in line with the reported increase of the intradiffusion coefficients for all considered alcohols upon their dilution. Further, the presence of hydrogen bonding clusters in the regarded mixtures was analyzed in detail employing molecular simulation techniques, cf. Fig. 5. The amount of alcohol molecules that do not participate in hydrogen bonding

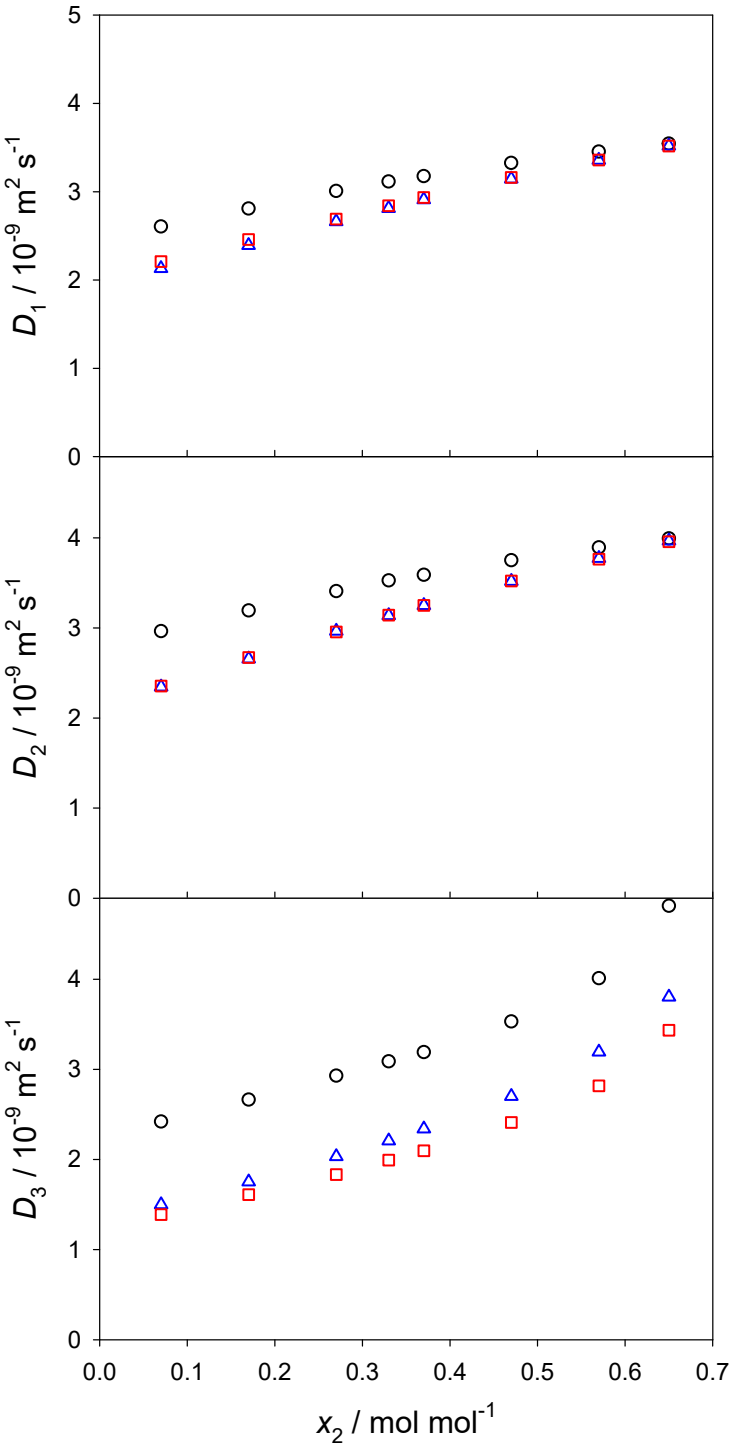

FIG. 4. Intradiffusion coefficient D_i of benzene (top), acetone (center) and an alcohol (bottom) of the ternary mixtures benzene + acetone + methanol (black) / ethanol (blue) / 2-propanol (red) at 298.15 K and 0.1 MPa along a constant benzene mole fraction path $x_1 = 0.33$ mol mol^{-1}. x_2 stands for the acetone mole fraction. Statistical uncertainties are within symbol size.

increases with decreasing alcohol mole fraction. In the alcohol-rich binary limit, about 70% of the alcohol molecules are self-associated trimers, as is the case for the pure alcohols. The amount of self-associated alcohol molecules forming trimers decreases with the reduction of the alcohol content. On the other hand, the amount of alcohol molecules forming dimers with another alcohol increases with decreasing alcohol content. The number of alcohol molecules hydrogen bonded to three or more partners is negligible. The amount of alcohol molecules that are hydrogen bonded to acetone was also determined.

C. Fick Diffusion Coefficient Matrix

The Fick diffusion matrix of the three ternary mixtures was measured by means of the Taylor dispersion technique. Numerical values of the matrix elements D_{ij}^V are reported in Table III. Further, in order to compare results from experiment and simulation, the measured Fick diffusion matrix in the volume-averaged reference frame $\boldsymbol{D}^V$ was converted into the molar-averaged reference frame $\boldsymbol{D}^M$ employing Eq. (4). For this conversion, the partial molar volumes have to be known. However, it can be shown for the regarded mixtures that the molar volumes of the pure liquids may be employed with negligible loss in conversion accuracy.

All experimental and simulation results for the ternary diffusion coefficients are consistent and their numerical values fulfill the theoretical restrictions given by Taylor and Krishna[40], i.e. the Fick diffusion matrix has positive and real eigenvalues, positive diagonal elements and a positive determinant. The eigenvalues, which are independent on the reference frame, are shown in Fig. 6, their numerical values are listed in the supplementary material. It can be seen that both eigenvalues grow monotonically with decreasing alcohol content for all three ternary mixtures. The larger eigenvalue $\hat{D}_1$ decreases in magnitude with increasing alcohol carbon chain length in the entire regarded composition range. The smaller eigenvalue $\hat{D}_2$ generally exhibits a similar behavior, i.e. it is larger for the shorter alcohols, however, the differences between the three mixtures are far less significant than for $\hat{D}_1$, cf. Fig. 6.

Fick diffusion coefficients are difficult to interpret from a physical perspective because they depend on hydrodynamic and thermodynamic contributions[37], cf. Eq. (8). For a better understanding of Fick diffusivity data, it is thus useful to analyze both contributions separately, i.e. the behavior of the thermodynamic factor matrix $\boldsymbol{\Gamma}$ and that of the phenomenological

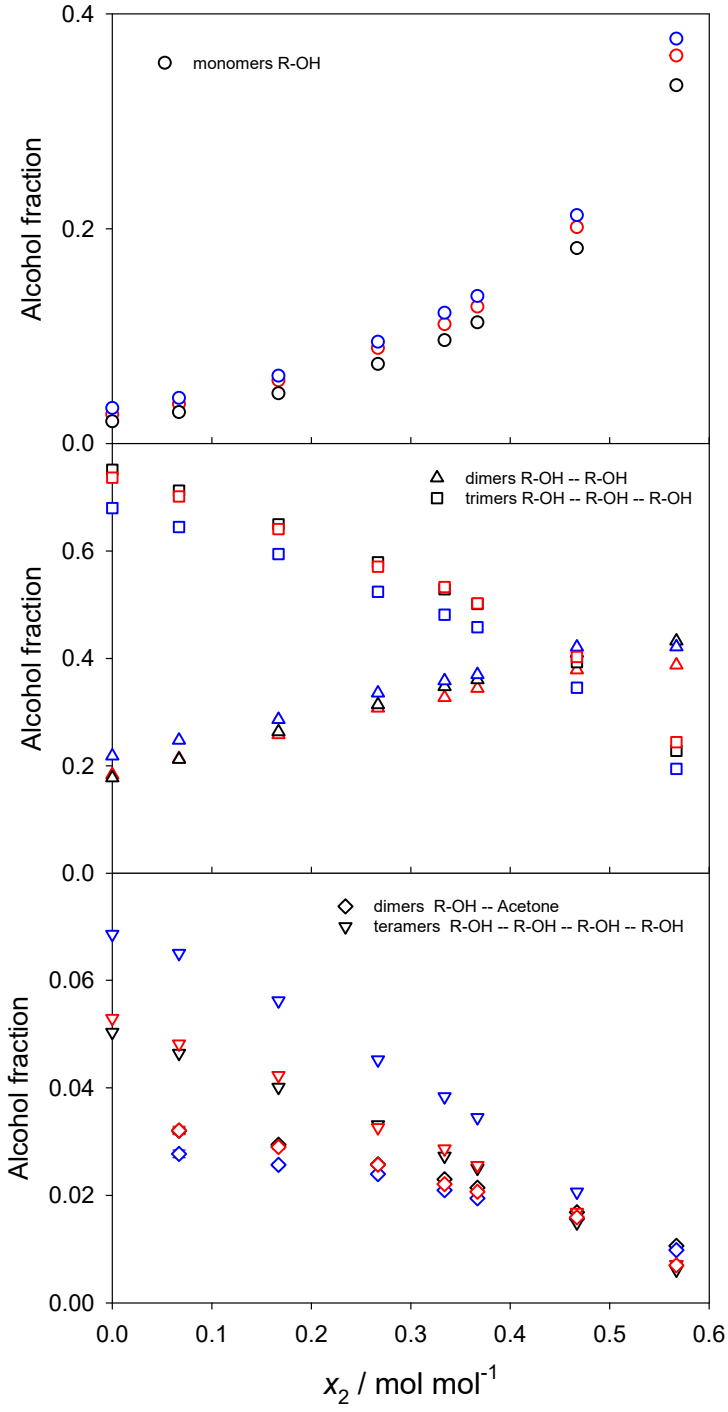

FIG. 5. Hydrogen bonding statistics of the ternary mixtures benzene + acetone + methanol (black) / ethanol (blue) / 2-propanol (red) at 298.15 K and 0.1 MPa along a constant benzene mole fraction path $x_1 = 0.33$ mol mol^{-1}. Calculated fractions of alcohol molecules forming hydrogen bonded monomers (top), dimers, trimers and tetramers (center and bottom) are shown. x_2 stands for the acetone mole fraction. Statistical uncertainties are within symbol size.

TABLE III. Experimental density ρ in kg m^{-3} and Fick diffusion coefficient data D_{ij}^V in 10^{-9}m^{2}s^{-1} with their uncertainties $\sigma/10^{-9}$m^{2}s^{-1} of the ternary mixtures benzene (1) + acetone (2) + methanol / ethanol / 2-propanol (3) at 298.15 K and 0.1 MPa along a constant benzene mole fraction path $x_1 = 0.33$ mol mol^{-1}.

benzene + acetone + methanol											
x_1	x_2	x_3	ρ	D_{11}^V	σ	D_{12}^V	σ	D_{21}^V	σ	D_{22}^V	σ
0.33	0.00	0.67	832.04	1.291	0.002						
0.33	0.07	0.60	831.25	1.409	0.054	−0.876	0.347	0.024	0.006	3.239	0.71
0.33	0.17	0.50	829.69	1.578	0.202	−0.799	0.228	0.062	0.057	3.371	0.197
0.33	0.27	0.40	827.73	1.760	0.098	−0.675	0.191	0.182	0.41	3.743	0.196
0.33	0.33	0.33	826.36	1.847	0.058	−0.823	0.153	0.332	0.056	3.878	0.100
0.33	0.37	0.30	825.56	1.954	0.065	−0.681	0.101	0.254	0.034	3.836	0.087
0.33	0.47	0.20	823.24	2.159	0.071	−0.225	0.029	1.590	0.125	4.350	0.091
0.33	0.57	0.10	820.74	2.241	0.067	−0.366	0.034	2.063	0.218	4.837	0.093
0.33	0.67	0.00	819.34							2.980	0.003
benzene + acetone + ethanol											
x_1	x_2	x_3	ρ	D_{11}^V	σ	D_{12}^V	σ	D_{21}^V	σ	D_{22}^V	σ
0.33	0.00	0.67	823.33	1.313	0.003						
0.33	0.07	0.60	823.03	1.411	0.072	−0.707	0.062	−0.163	0.015	2.596	0.053
0.33	0.17	0.50	822.36	1.602	0.028	−0.651	0.033	−0.204	0.017	2.822	0.041
0.33	0.27	0.40	821.61	1.731	0.038	−0.641	0.034	−0.155	0.010	3.078	0.032
0.33	0.33	0.33	821.08	1.781	0.042	−0.667	0.027	0.036	0.003	3.275	0.029
0.33	0.37	0.30	820.78	1.769	0.039	−0.648	0.047	0.286	0.019	3.497	0.079
0.33	0.47	0.20	819.91	1.910	0.088	−0.731	0.062	0.493	0.037	3.870	0.098
0.33	0.57	0.10	819.02	2.397	0.087	−0.506	0.051	0.903	0.043	4.199	0.072
0.33	0.67	0.00	818.34							2.980	0.003
benzene + acetone + 2-propanol											
x_1	x_2	x_3	ρ	D_{11}^V	σ	D_{12}^V	σ	D_{21}^V	σ	D_{22}^V	σ
0.33	0.00	0.67	812.80	1.124	0.002						
0.33	0.07	0.60	812.99	1.270	0.072	−0.539	0.041	−0.137	0.009	2.201	0.054
0.33	0.17	0.50	813.33	1.390	0.066	−0.567	0.047	−0.142	0.010	2.526	0.038
0.33	0.27	0.40	813.82	1.594	0.042	−0.461	0.031	−0.374	0.021	2.708	0.032
0.33	0.33	0.33	814.23	1.747	0.041	−0.323	0.027	−0.284	0.019	2.969	0.059
0.33	0.37	0.30	814.48	1.827	0.059	−0.376	0.044	−0.298	0.027	3.090	0.098
0.33	0.47	0.20	815.39	2.034	0.101	−0.195	0.022	−0.189	0.027	3.420	0.125
0.33	0.57	0.10	816.58	2.349	0.092	−0.076	0.013	0.366	0.041	3.933	0.138
0.33	0.67	0.00	818.34							2.980	0.003

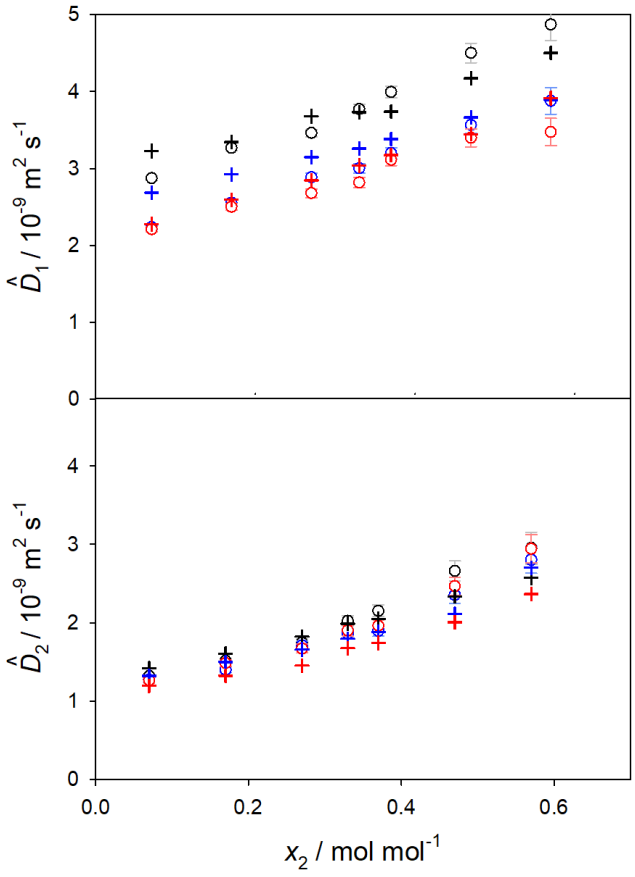

FIG. 6. First (top) and second (bottom) eigenvalue of the Fick diffusion coefficient matrix **D** of the ternary mixtures benzene (1) + acetone (2) + methanol (black) / ethanol (blue) / isopropanol (red) (3) at 298.15 K and 0.1 MPa along a constant benzene mole fraction path $x_1 = 0.33$ mol mol^{-1}. x_2 stands for the acetone mole fraction. Data from present experiments (+) are compared with present simulation results (∘).

coefficient matrix **Δ**. The composition dependence of the Fick diffusion coefficients D_{ij}^M, the thermodynamic factor elements Γ_{ij} and the phenomenological coefficients Δ_{ij} is shown in Figs. 7 to 10.

Both main elements of the Fick diffusion coefficient matrix increase with falling alcohol content. In general, $D_{11}^M < D_{22}^M$, which is expected because of the size difference between benzene and acetone molecules. However, the most striking feature is the insensitivity of D_{11}^M on the alcohol carbon chain length, which is especially visible at high alcohol concentrations. On the other hand, the hydrodynamic behavior given by the phenomenological coefficient Δ_{11} does depend on the alcohol type, i.e. Δ_{11} of the ternary mixture involving methanol is

significantly larger than that of the other two mixtures, which is consistent with a smaller diffusion size of methanol, cf. Fig. 7. In contrast, the thermodynamic factor Γ_{11} of the ternary mixture with methanol is lower than that of the mixtures with ethanol or 2-propanol. From Eq. (8), $D_{11}^M = \Delta_{11}\Gamma_{11} + \Delta_{12}\Gamma_{21}$. Because the major contribution to D_{11}^M stems from the first term, i.e. the second term yields at most 12% of the total, it is clear that the observed independence of D_{11}^M on the alcohol type has its root in the factorization of the hydrodynamics and non-ideal thermodynamics.

As can be seen in Fig, 8, D_{22}^M decreases with carbon chain length of the alcohol in the ternary mixture, i.e. methanol > ethanol > 2-propanol. Δ_{22} shows a similar behavior, but exhibits a maximum for all mixtures at acetone mole fractions $x_2 \approx 0.47$ mol mol^{-1}. This suggests a change in hydrodynamics, i.e. diffusion size, at this composition. The thermodynamic factor Γ_{22} goes through a minimum close to equimolar composition and has a strong composition dependence when the alcohol mole fraction decreases. Further, the lowest value corresponds to the ternary mixture containing 2-propanol and not methanol as for Γ_{11}.

The cross elements of the Fick diffusion matrix are shown in Figs. 9 and 10. D_{12}^M, which relates the mass flux of benzene to the acetone concentration gradient, is negative and smaller than the main elements of all regarded mixtures. Nonetheless, for the highest alcohol concentration, the ratio $|D_{12}^M/D_{11}^M|$ reaches 0.5, suggesting a non-negligible coupling between acetone concentration with the mass flux of benzene for these ternary mixtures. A negative cross element of the diffusion matrix D_{ij} implies that species i diffuses towards larger concentrations of species j. D_{21}^M shows a stronger composition dependence, especially for acetone mole fractions $x_2 > 0.3$ mol mol^{-1}. For all ternary mixtures, D_{21}^V has positive or negative values depending on acetone mole fraction. Further, $|D_{21}^M|$ is usually significantly smaller than its corresponding main coefficient D_{22}^M. On the other hand, both phenomenological cross coefficients Δ_{12} and Δ_{21} are positive and exhibit larger values for the ternary mixture with methanol due to its smaller diffusion size. Again, a maximum of the phenomenological coefficient Δ_{21} was observed at $x_2 \approx 0.47$ mol mol^{-1}. The main feature of the cross terms of the thermodynamic coefficient matrix Γ_{12} and Γ_{21} is that they may acquire negative values. In fact, the cross elements D_{ij}^M acquire negative values when Γ_{ij} is negative and $\Gamma_{ij}\Delta_{ii} > \Gamma_{jj}\Delta_{ij}$. Therefore, negative values of D_{12}^M and D_{12}^M are mainly a consequence of the non-ideal thermodynamic behavior of the ternary mixtures.

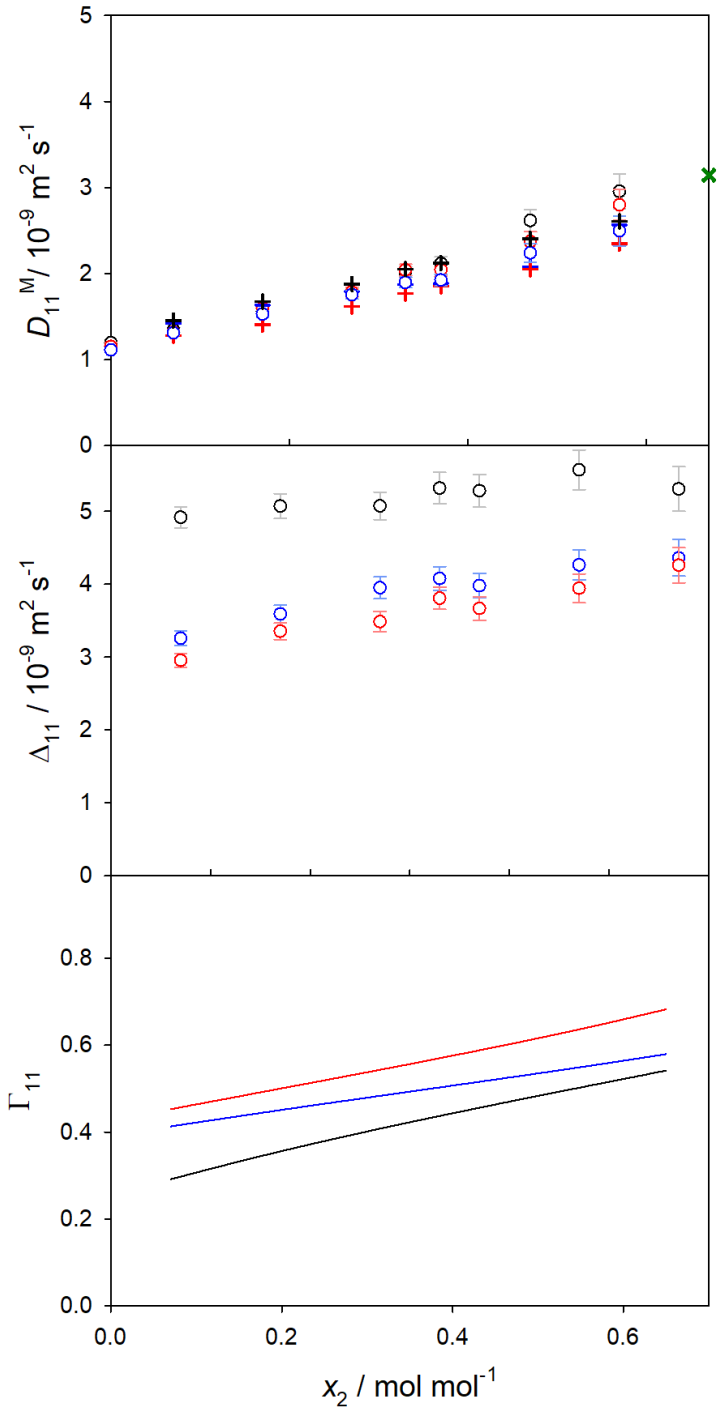

FIG. 7. Fick diffusion coefficient D_{11}^{M} (top), phenomenological coefficient Δ_{11} (center) and thermodynamic factor element Γ_{11} (bottom) of the ternary mixtures benzene (1) + acetone (2) + methanol (black) / ethanol (blue) / 2-propanol (red) (3) at 298.15 K and 0.1 MPa along a constant benzene mole fraction path $x_1 = 0.33$ mol mol^{-1}. The green cross indicates asymptotic values approaching the binary subsystem. x_2 stands for the acetone mole fraction. Data from present experiments (+) are compared with present simulation results (○).

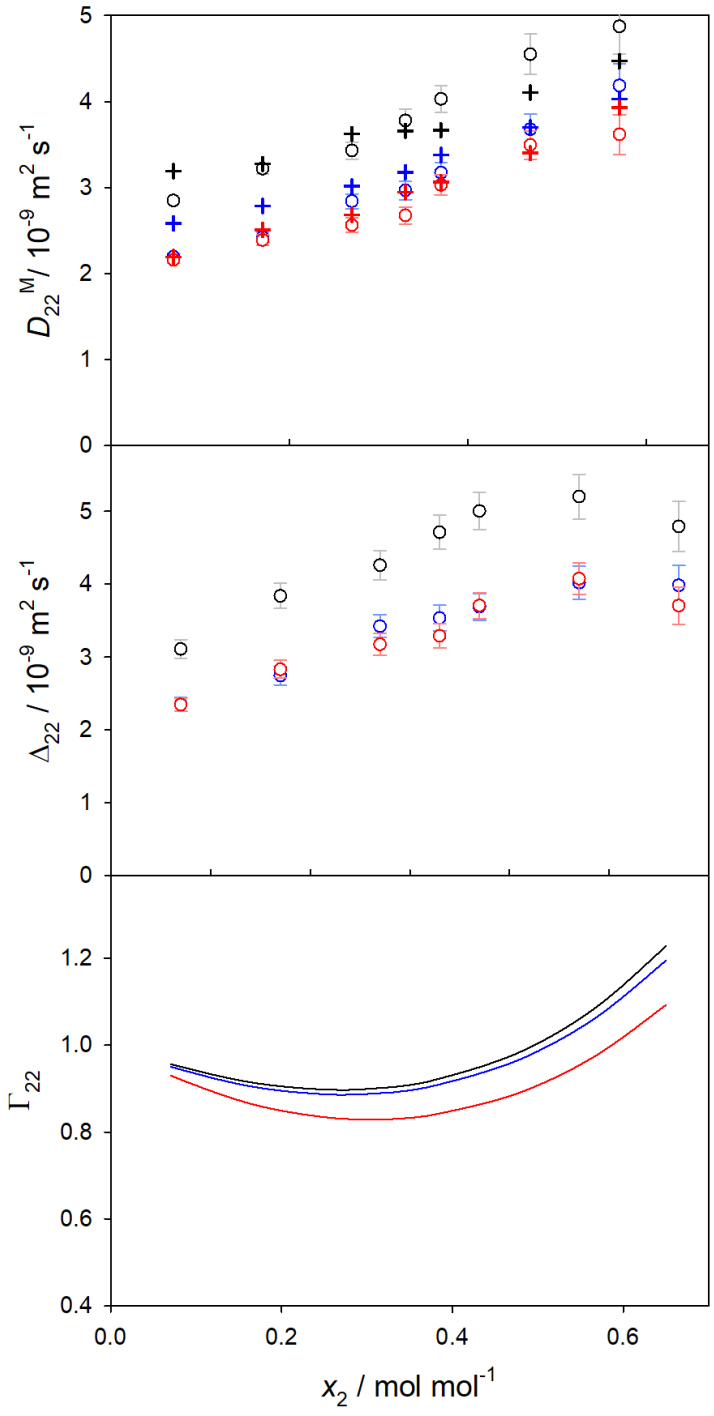

FIG. 8. Fick diffusion coefficient D_{22}^{M} (top), phenomenological coefficient Δ_{22} (center) and thermodynamic factor element Γ_{22} (bottom) of the ternary mixtures benzene (1) + acetone (2) + methanol (black) / ethanol (blue) / 2-propanol (red) (3) at 298.15 K and 0.1 MPa along a constant benzene mole fraction path $x_1 = 0.33$ mol mol^{-1}. x_2 stands for the acetone mole fraction. Data from present experiments (+) are compared with present simulation results (∘).

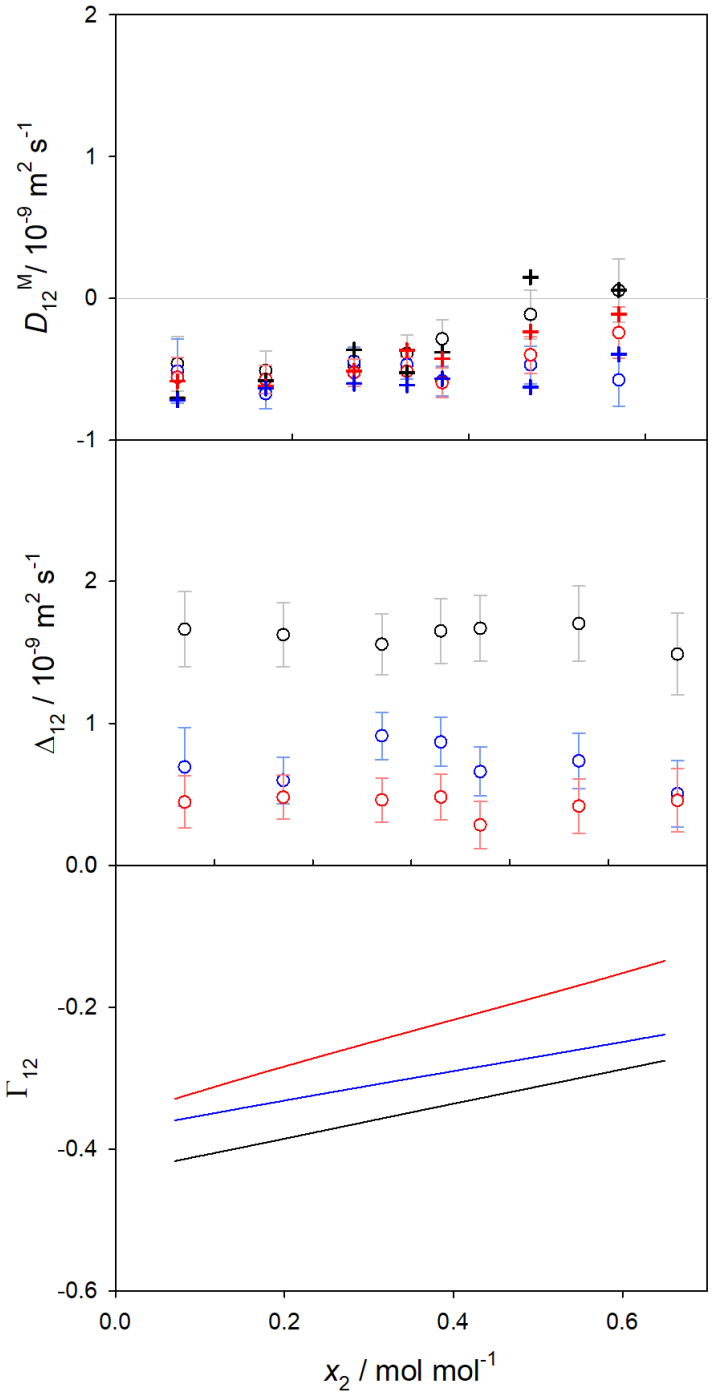

FIG. 9. Fick diffusion coefficient D_{12}^{M} (top), phenomenological coefficient Δ_{12} (center) and thermodynamic factor element Γ_{12} (bottom) of the ternary mixtures benzene (1) + acetone (2) + methanol (black) / ethanol (blue) / 2-propanol (red) (3) at 298.15 K and 0.1 MPa along a constant benzene mole fraction path $x_1 = 0.33$ mol mol^{-1}. x_2 stands for the acetone mole fraction. Data from present experiments (+) are compared with present simulation results (○).

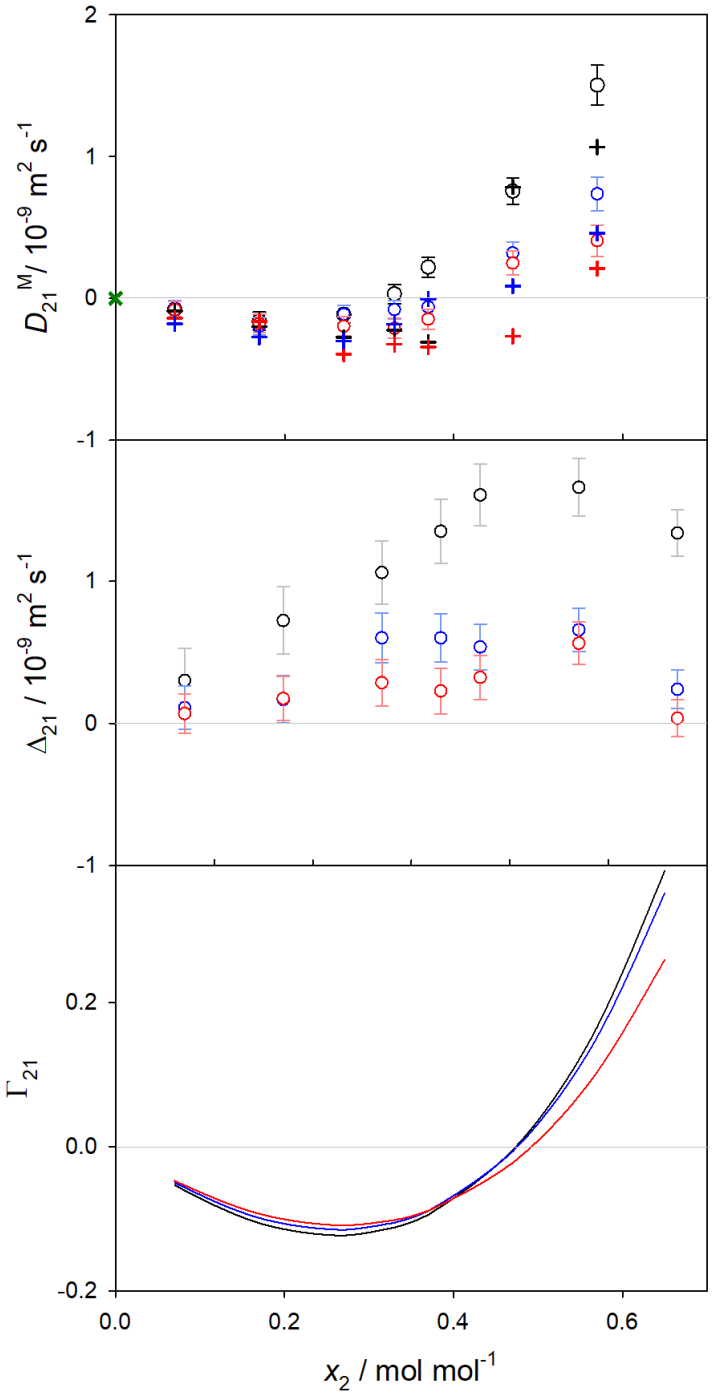

FIG. 10. Fick diffusion coefficient D_{21}^{M} (top), phenomenological coefficient Δ_{21} (center) and thermodynamic factor element Γ_{21} (bottom) of the ternary mixtures benzene (1) + acetone (2) + methanol (black) / ethanol (blue) / 2-propanol (red) (3) at 298.15 K and 0.1 MPa along a constant benzene mole fraction path $x_1 = 0.33$ mol mol^{-1}. The green cross indicates asymptotic values approaching the binary subsystem. x_2 stands for the acetone mole fraction. Data from present experiments (+) are compared with present simulation results (○).

Thermodynamics and hydrodynamics and of liquid mixtures, and hence the thermodynamic factor and the phenomenological coefficient matrices, are highly influenced by the presence of hydrogen bonding. To elucidate this issue, molecular simulation techniques were employed to analyze self-associated alcohol clusters. The amount of alcohol monomers, hydrogen bonded dimers, trimers and tetramers that are present in the studied ternary mixtures are shown in the supplementary material. It can be seen that the fraction of alcohol molecules in monomeric form increases upon their dilution. In the alcohol-rich binary limit $x_2 \to 0$, about 70% of the alcohol molecules are part of self-associated trimers, as is the case for the pure alcohols. The amount of self-associated alcohol molecules forming trimers decreases with the reduction of alcohol content, which can be explained by the limited availability of partner molecules that can participate in hydrogen bonding. On the other hand, the fraction of alcohol molecules forming dimers increases with decreasing alcohol content. Almost the same amount of alcohol dimers and trimers is present in all studied ternary mixtures at $x_2 = 0.47$ mol mol^{-1}, which corresponds to the maximum of Δ_{22} and Δ_{21}. For higher acetone mole fractions, the amount of dimers exceeds that of trimers. Thus, a relation between these changes in alcohol cluster size distribution and hydrodynamic behavior of the elements of the phenomenological matrix involving acetone can be inferred for the studied ternary mixtures.

Binary Subsystems

To better appreciate the direct influence of the thermodynamic factor on Fick diffusivity in ternary mixtures, it is compelling to consider diffusion in the conceptually more simple binary subsystems. The subsystems benzene + alcohol are of particular interest because their binary Fick diffusion coefficient D behaves similarly to the main term of the ternary Fick diffusion coefficient matrix D_{11}^M, i.e. D does not depend on the alcohol type, especially at alcohol mole fractions below 0.7 mol mol^{-1}, cf. Fig. 11.

For all three binary mixtures, the binary Fick diffusion coefficient shows a strong mole fraction dependence. When an alcohol (R-OH) is infinitely diluted in benzene, i.e. $x_{\mathrm{R-OH}} \to 0$, the Fick diffusion coefficient is higher than that of the self-diffusion coefficient of the pure liquid, suggesting hydrogen bond breaking because of the dominating presence of benzene. However, when the alcohol mole fraction reaches $x_{\mathrm{R-OH}} \geq 0.2$ mol mol^{-1}, the binary Fick

diffusion coefficient decreases to less than half of its infinite dilution value, indicating the presence of organized alcohol microstructures caused by association effects due to hydrogen bonding.

In binary mixtures, the Fick diffusion coefficient D is directly related to the corresponding MS diffusion coefficient $Đ$ by

$$D = \Gamma Đ, \tag{28}$$

where the thermodynamic factor Γ is a scalar quantity given by Eq. (9). In analogy to the corresponding phenomenological coefficients of ternary mixtures, cf. Eq. (8), the binary MS diffusion coefficient and the thermodynamic factor represent the hydrodynamic and thermodynamic contributions to diffusion. As can be seen in Fig. 11, the MS diffusion coefficient of the benzene + alcohol mixtures does depend on the alcohol type. For instance, the binary MS diffusion coefficient of benzene + methanol is significantly larger than that of the binary mixture with 2-propanol, which is the expected hydrodynamic behavior because of the difference in molecular size. In contrast, the thermodynamic factor Γ of the binary mixture of benzene with methanol is lower than that of the mixtures with ethanol or 2-propanol. Further, the composition dependence of the binary MS diffusion coefficient shows a maximum for the three binary mixtures at $x_{\mathrm{R-OH}} \approx 0.2$ mol mol^{-1}, which has been related to microscopic clustering due to alcohol self-association[48,62]. The presence of a thermodynamic factor minimum at the same composition confirms the interdependence between hydrodynamics and thermodynamics of liquid mixtures. In fact, the pronounced composition dependence of the thermodynamic factor and its values far from unity indicate the presence of strong non-idealities, which are expected to be more important for the binary mixture involving methanol and are related to the presence of clusters and micro-heterogeneity. Thus, as in the case of the ternary mixtures, a trade-off between the hydrodynamic and thermodynamic contributions to the Fick diffusion coefficient causes the observed insensitivity of D on the alcohol type.

At this point, the question arises whether a direct correlation between the observed alcohol type independence of the Fick diffusion coefficient in the binary limit of the mixture benzene + alcohol and the main term D_{11} of the ternary benzene + acetone + alcohol exists. To investigate this issue, additional molecular dynamics simulations were performed along neighboring constant benzene mole fraction paths $x_1 = 0.1$ and 0.2 mol mol^{-1}. From the

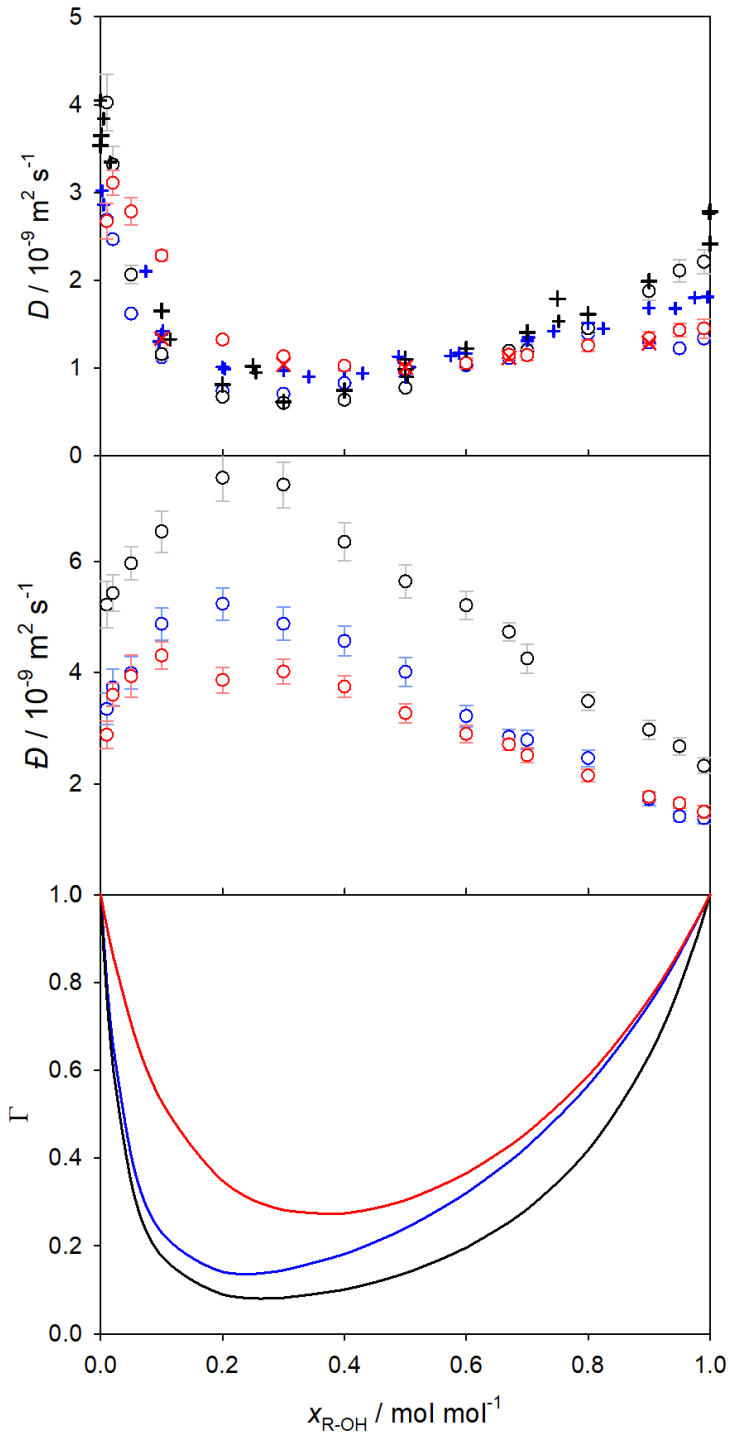

FIG. 11. Binary Fick D (top), Maxwell-Stefan $Đ$ diffusion coefficient (center) and thermodynamic factor (bottom) of the binary mixtures benzene + methanol (black) / ethanol (blue) / 2-propanol (red) at 298.15 K and 0.1 MPa. Where possible, molecular simulation results (○) are compared with present measurements (x) and experimental data from the literature[15,16,19,23,62] (+). $x_{\mathrm{R-OH}}$ stands for the alcohol mole fraction.

binary limit $x_2 \to 0$, it is expected that these ternary mixtures show different values for D_{11}^M in case of the ternary mixtures involving methanol or ethanol, which was confirmed by the molecular simulation results, cf. supplementary material.

D. Maxwell-Stefan Diffusion Coefficient Matrix

MS diffusion coefficients are interesting to analyze because they can be the subject of physical interpretation in terms of intermolecular friction or drag[40] and because of the unexpected behavior of one of the main elements of the Fick diffusion coefficient matrix. The three independent MS diffusion coefficients $Đ_{ij}$ of the three studied ternary mixtures obtained from equilibrium molecular dynamics and the Green-Kubo formalism are shown in Fig. 12. Their numerical values are listed in the supplementary material.

The behavior of the three MS diffusion coefficients is different. $Đ_{12}$ shows a rather monotonic growth similar to that observed for the main Fick diffusion coefficients. Moreover, as for D_{11}, the numerical values of $Đ_{12}$ are also independent on the alcohol type. This indicates that the frictional drag between benzene and acetone is alike for the mixtures involving different alcohols. Thus, it can be inferred that the microscopic arrangement and collective intermolecular interactions between benzene and acetone molecules are comparable in the three ternary mixtures. $Đ_{13}$, characterizing the drag between benzene and the alcohol, also increases with decreasing alcohol content in the mixture. Further, its numerical value depends on alcohol type, i.e. $Đ_{13}$ increases with decreasing carbon chain length of the alcohol. Such a behavior was also observed for $Đ_{23}$, however, its composition dependence shows a maximum at an acetone mole fraction $x_2 \approx 0.4$ mol mol^{-1} for all ternary mixtures. Note that the values of the MS diffusion coefficients involving an alcohol, i.e. $Đ_{13}$ and $Đ_{23}$, are much larger than $Đ_{12}$, suggesting the presence of significantly stronger intermolecular drag effects.

E. Radial Distribution Functions

To gain a better understanding of the intermolecular interactions and microscopic structure that lead to the observed diffusion coefficients, RDF were analyzed. Fig. 13 shows the RDF of the studied mixtures at equimolar composition, i.e. $x_1 = x_2 = x_3 = 1/3$ mol

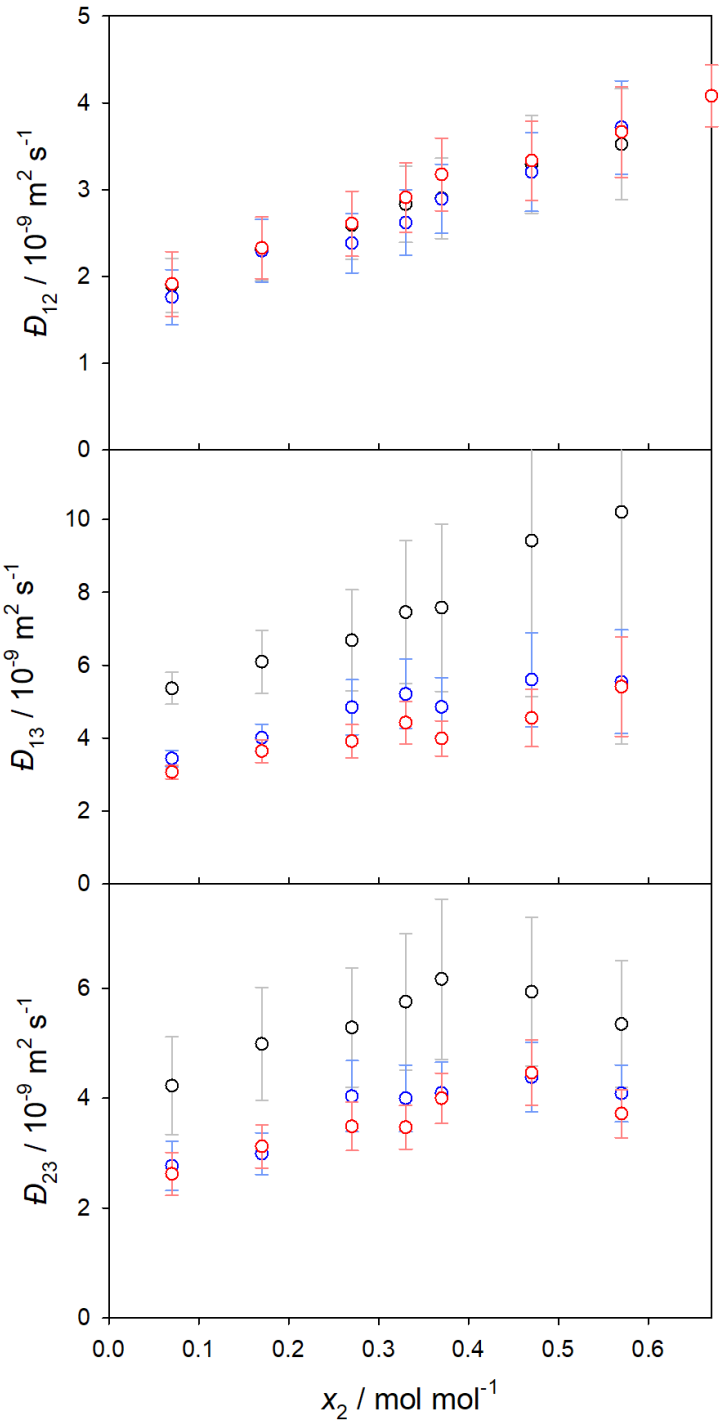

FIG. 12. Maxwell-Stefan diffusion coefficients between components 1 and 2 (top), 1 and 3 (center) as well as 2 and 3 (bottom) of the ternary mixtures benzene (1) + acetone (2) + methanol (black) / ethanol (blue) / 2-propanol (red) (3) at 298.15 K and 0.1 MPa along a constant benzene mole fraction path $x_1 = 0.33$ mol mol^{-1} from molecular simulation. x_2 stands for the acetone mole fraction.

mol^{-1}, for the interactions between the aromatic carbons of benzene and the methyl group of the alcohols and acetone. The benzene-benzene RDF exhibits a double peak with maxima at approximately 5.0 and 6.3 Å. This peak bifurcation is due to the presence of different preferred spatial configurations of benzene molecules within their first solvation shell. The location and shape of this double peak corresponds to that of the pure liquid, thus, the local environment of benzene molecules located in the first solvation shell is largely preserved in the ternary mixtures. This suggests the presence of segregated benzene clusters, which is in line with the findings of Požar et al.[28]. Further, this near-neighbor structure is almost identical for all studied mixtures, regardless of alcohol type. A similar behavior was observed for $g_{\mathrm{CH-CH3}}(r)$ between benzene and acetone, i.e. the density of the acetone methyl groups located within the first solvation shell of benzene remains more or less constant, independent of alcohol type. The maxima of the first, second and third peaks are located at $\sim$ 3.9, 5.9 and 8.2 Å , respectively. This suggests that the polar interactions between acetone and benzene[30] are affected in the same way by the presence of an alcohol. To some extent, this observation explains the lack of sensitivity of the ternary MS diffusion coefficient $Đ_{12}$ on alcohol type.

The RDF of the interaction between benzene and the non-polar methyl group of the three alcohols exhibit, as expected, a different behavior for each alcohol. The first peak is located between 4.0 and 4.2 Å for methanol to 2-propanol, respectively. Further, the ternary mixture with methanol has a rather well-defined first peak, whereas the mixtures involving ethanol and 2-propanol show a broader and split first peak due to configurational differences. Note that the magnitude of the main peaks of the three RDF in Fig. 13 is similar so that a clear preference of benzene for the type of their surrounding molecules cannot be assigned.

In Fig. 14, selected RDF for acetone as a central molecule are depicted. The acetone-acetone RDF $g_{\mathrm{CH3-CH3}}(r)$ has two peaks at short distances with maxima at approximately 4.0 and 5.7 Å, which is due to the presence of two equivalent methyl groups constituting the acetone molecule. Acetone also contains a carbonyl group, hence it is able to associate through dipole-dipole interactions[30]. This interaction is characterized by $g_{\mathrm{O-CH3}}(r)$, which shows a well-defined first peak located at $\sim$ 3.6 Å, followed by two small peaks. Because the magnitude of this first peak is higher than that of $g_{\mathrm{CH3-CH3}}(r)$, it can be concluded that the probability of finding an acetone oxygen around an acetone methyl group is higher than finding an acetone methyl group. As in case of benzene, it should be noticed that

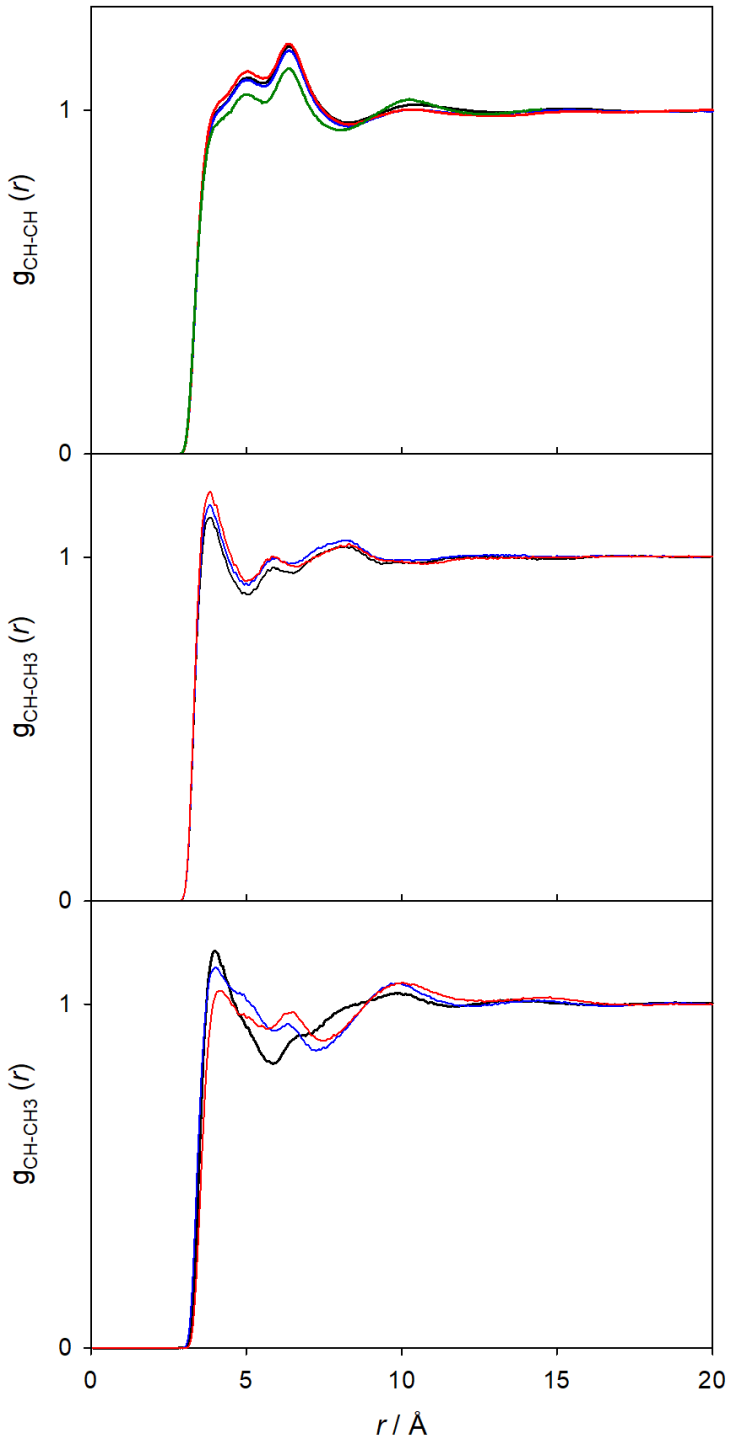

FIG. 13. Radial distribution functions of the benzene-benzene $g_{\mathrm{CH-CH}}(r)$ (top), benzene-acetone $g_{\mathrm{CH-CH3}}(r)$ (center) and benzene-alcohol $g_{\mathrm{CH-CH3}}(r)$ (bottom) interactions of the equimolar ternary mixtures benzene + acetone + methanol (black) / ethanol (blue) / 2-propanol (red) at 298.15 K and 0.1 MPa. The green line represents the RDF of benzene in its pure state.

the major features of $g_{\mathrm{CH3-CH3}}(r)$ and $g_{\mathrm{O-CH3}}(r)$, i.e. location and shape of the peaks, for pure acetone are conserved in the mixture, suggesting the presence of segregated acetone pockets[28]. The smaller magnitude of the pure component's first peak can be attributed to statistical standardization due to better homogeneity. The cross interaction acetone-alcohol given by $g_{\mathrm{CH3-CH3}}(r)$ yields a different picture. This RDF depends on the alcohol type, the peaks change in magnitude, shape and position, indicating strong differences in the near-neighbor structure of the different alcohol molecules around acetone. E.g., in the ternary mixture with methanol, more alcohol molecules can be found in the first solvation shell than is the case for the ternary mixtures with ethanol or 2-propanol.

The RDF $g_{\mathrm{OH-O}}(r)$ and $g_{\mathrm{O-O}}(r)$ of the alcohol-alcohol interaction are typical for hydrogen bonding molecules, i.e. $g_{\mathrm{OH-O}}$ has a sharp and very pronounced first peak at ~ 1.9 Å, followed by a smaller second peak located at ~ 3.4 Å, cf. Fig. 15. These peaks vary in magnitude for the different alcohols and, at distances beyond 4 Å, there are also changes in peak location or shape. Note that the magnitudes of the main RDF peaks of $g_{\mathrm{OH-O}}(r)$ and $g_{\mathrm{O-O}}(r)$ are significantly larger than those of the RDF related to benzene or acetone, indicating that the well-defined hydrogen bonding structure of the alcohols persists in the ternary mixture. This induces local segregation as reported for binary mixtures of alcohols with alkanes[28,29].

The RDF between the hydrogen of the alcohol hydroxyl group and the oxygen of the acetone carbonyl group $g_{\mathrm{OH-O}}(r)$ is shown in Fig. 15. Although the acetone oxygen may have the ability to accept hydrogen bonds[24], practically no hydrogen bond formation between acetone and alcohol molecules was found in the studied ternary mixtures. The observed first peak of $g_{\mathrm{OH-O}}(r)$ is located at ≈ 3.6 Å and has a magnitude that is more than eight times smaller than that describing alcohol-alcohol hydrogen bonding. Thus, as expected, alcohol molecules prefer self-association through hydrogen bonding to association with acetone. Further, because of the substantial strength of the hydrogen bonding network, acetone molecules do not sequester alcohol molecules and they neither brake nor increase the alcohol hydrogen bond network[24]. For instance, the calculated amount of alcohol molecules hydrogen bonded to acetone is below 3% for the constant benzene composition path $x_1 = 0.33$ mol mol^{-1}.

F. Microscopic Structure

Observations of the macroscopic properties, hydrogen bonding and RDF suggest the presence of micro-heterogeneity in the studied ternary mixtures. Microscopic inhomogeneity has already been observed for the binary mixtures of ethanol + acetone[63] and ethanol + benzene[29]. A valid method to detect the presence of microscopic segregation and long-range clustering is the visual examination of molecular configurations. Clearly, the presence of inhomogeneous mixing was confirmed. Further, the hydrogen bonded structures formed by alcohol molecules span through the entire simulation volume, causing the formation of segregation pockets. Selected snapshots of the simulation volume for the equimolar ternary mixtures are shown in Fig. 16.

VI. CONCLUSION

The Fick diffusion coefficient matrix of three ternary mixtures of benzene + acetone + methanol / ethanol / 2-propanol was measured with the Taylor dispersion technique along the constant benzene mole fraction path $x_1 = 0.33$ mol mol^{-1}.

Unexpected features of the Fick diffusion coefficient matrix were found:

- The main element D_{11}^M is almost independent on the alcohol chain length.
- The smaller eigenvalue $\hat{D}_2$ shows only a slight dependence on the alcohol type.

Because of the challenging conceptual interpretation of the Fick diffusion coefficient matrix, these features were analyzed in terms of the hydrodynamic and thermodynamic contributions to diffusion, employing molecular dynamics simulation techniques. It was found that the hydrodynamic and thermodynamic contributions to the Fick diffusion coefficient do show, as expected, a dependence on the alcohol. In the case of the main diffusion coefficient D_{11}^M, a trade-off between the major hydrodynamic and thermodynamic contributions leads to the observed alcohol type independence. It was shown how the presence of alcohol clusters governs the observed hydrodynamic and thermodynamic behavior of the studied ternary mixtures. Further, the fact that the Fick diffusion coefficient of the binary subsystems benzene + methanol / ethanol / 2-propanol does not change in most of the composition range, indicates a relation between the Fick diffusion coefficients of the ternary mixture with that of its binary limits.

Another interesting finding is that the Maxwell-Stefan diffusion coefficient between benzene and acetone is also insensitive to the alcohol carbon chain length, which can be interpreted as a consequence of the presence of similar microscopic arrangements and collective intermolecular interactions between benzene and acetone molecules in the three ternary mixtures.

From the hydrogen bonding statistics and RDF analyses, it was shown that alcohol molecules self-associate to form clusters, induce segregation and thus microheterogeneity.

SUPPLEMENTARY MATERIAL

See supplementary material for hydrogen bonding statistics, simulation details and numerical simulation results.

ACKNOWLEDGMENTS

This work was funded by the Deutsche Forschungsgemeinschaft (DFG) under the grant VR 6/11-1. The simulations were carried out on the national supercomputer Hazel hen at the High Performance Computing Center Stuttgart (HLRS) within the project MMHBF2.

REFERENCES

REFERENCES

[1]T. M. Koller, J. Ramos, P. Schulz, I. G. Economou, M. H. Rausch, and A. P. Fröba, J. Phys. Chem. B **121**, 4145 (2017).

[2]S. L. Chin, Q. Lu, E. L. Dane, L. Dominguez, C. J. McKnight, J. E. Straub, and M. W. Grinstaff, J. Am. Chem. Soc. **138**, 6532 (2016).

[3]G. Guevara-Carrion, Y. Gaponenko, T. Janzen, J. Vrabec, and V. Shevtsova, J. Phys. Chem. B **120**, 12193 (2016).

[4]X.-Y. Wang, R. D. Raharjo, H. J. Lee, Y. Lu, B. D. Freeman, and I. C. Sanchez, J. Phys. Chem. B **110**, 12666 (2006).

[5]K. Polok, W. Gadomski, F. Sokolić, and L. Zoranić, J. Mol. Liq. **159**, 60 (2011).

[6]D. Babic and A. Pfennig, Fluid Phase Equilib. **245**, 140 (2006).

[7]D. G. Miller, J. Phys. Chem. **90**, 1509 (1986).

[8]J. C. Legros, Y. Gaponenko, A. Mialdun, T. Triller, A. Hammon, C. Bauer, W. Kohler, and V. Shevtsova, Phys. Chem. Chem. Phys. **17**, 27713 (2015).

[9]V. Sechenyh, J. C. Legros, A. Mialdun, J. M. Ortiz de Zárate, and V. Shevtsova, J. Phys. Chem. B **120**, 535 (2016).

[10]P. J. Dunlop and L. J. Gosting, J. Am. Chem. Soc. **77**, 5238 (1955).

[11]A. E. Fick, Pogg. Ann. Phys. Chem. **94**, 59 (1855).

[12]U. K. Padidela, T. Khana, and R. N. Behera, Phys. Chem. Liq. , 1 (2017), https://doi.org/10.1080/00319104.2017.1407932.

[13]T. Janzen, Y. Gaponenko, A. Mialdun, G. Guevara-Carrion, J. Vrabec, and V. Shevtsova, RSC Adv. **8**, 10017 (2018).

[14]P. S. Nikam and N. P. Nikam, Int. J. Chem. Sci. **2**, 603 (2004).

[15]A. Alimadadian and C. P. Colver, Can. J. Chem. Eng. **54**, 208 (1976).

[16]M. Zhou, X. Yuan, Y. Zhang, and K. T. Yu, Ind. Eng. Chem. Res. **52**, 10845 (2013).

[17]D. W. McCall and D. C. Douglass, J. Phys. Chem. **71**, 987 (1967).

[18]C. C. Caldwell and A. L. Baab, J. Phys. Chem. **59**, 1113 (1955).

[19]D. K. Anderson, J. R. Hall, and A. L. Babb, J. Phys. Chem. **62**, 404 (1958).

[20]P. A. Johnson and A. L. Babb, J. Chem. Phys. **60**, 14 (1956).

[21]P. A. Johnson and A. L. Babb, Chem. Rev. **56**, 387 (1956).

[22]D. T. Jamieson and J. B. Irving, Adv. Therm. Cond. **13**, 185 (1974).

[23]S. S. Rao and C. O. Bennett, AIChE J. **17**, 75 (1971).

[24]J. J. Max and C. Chapados, J. Chem. Phys. **122**, 014504 (2005).

[25]A. Perera, L. Zoranić, F. Sokolić, and R. Mazighi, J. Mol. Liq. **159**, 52 (2011).

[26]D. L. Jadhav, N. K. Karthick, P. P. Kannan, R. Shanmugam, A. Elagovan, and G. Arivazhagan, J. Mol. Struct. **1130**, 497 (2017).

[27]J. J. Guitiérrez-Sevillano, S. Calero, and R. Krishna, Phys. Chem. Chem. Phys. **17**, 20114 (2015).

[28]M. Požar, J.-B. Seguier, J. Guerche, R. Mazighi, L. Zoranić, M. Mijaković, B. Kežić-Lovrinčević, F. Sokolić, and A. Perera, Phys. Chem. Chem. Phys. **17**, 9885 (2015).

[29]M. Požar, B. Lovrinčević, L. Zoranić, T. Primorac, F. Sokolić, and A. Perera, Phys. Chem. Chem. Phys. **18**, 23971 (2016).

[30]R. Kumar, S. Jayakumar, and V. Kannappan, Indian J. Pure App. Phys. **46**, 169 (2008).

[31]G. Matisz, A. M. Kelterer, W. M. F. Fabian, and S. Kunsági-Máté, J. Phys. Chem. A **115**, 10556 (2011).

[32]S. Parez, G. Guevara-Carrion, H. Hasse, and J. Vrabec, Phys. Chem. Chem. Phys. **15**, 3985 (2013).

[33]X. Liu, S. K. Schnell, J.-M. Simon, D. Bedeaux, S. Kjelstrup, A. Bardow, and T. J. H. Vlugt, J. Phys. Chem. B **115**, 12921 (2011).

[34]X. Liu, C. Martín, E. McGarrity, S. K. Schnell, S. Calero, J. M. Simon, D. Bedeaux, S. Kjelstrup, A. Bardow, and T. J. H. Vlugt, Ind. Eng. Chem. Res. **51**, 10247 (2012).

[35]N. Sohrevardi, M. R. Bozorgmehr, and M. M. Heravi, J. Supercrit. Fluids **130**, 321 (2017).

[36]E. L. Cussler, *Mass Transfer in Fluid Systems*, 2nd ed. (Cambridge University Press, Cambridge, 1997).

[37]D. Buzatu, F. D. Buzatu, L. Paduano, and R. Sartorio, J. Solution Chem. **36**, 1373 (2007).

[38]J. Yan, S. Le, and X. Luo, Adv. Nat. Sci. **1**, 24 (2008).

[39]W. E. Price, J. Chem. Soc. Faraday Trans. 1 **84**, 2431 (1988).

[40]R. Taylor and R. Krishna, *Multicomponent Mass Transfer* (John Wiley & Sons, New York, 1993).

[41]D. Matuszak, G. L. Aranovich, and M. D. Donohue, J. Non-Equil. Thermodyn. **31**, 355 (2006).

[42]R. Krishna, Chem. Soc. Rev. **44**, 2812 (2015).

[43]R. Krishna and J. M. van Baten, Ind. Eng. Chem. Res. **44**, 6939 (2005).

[44]D. G. Leaist, J. Chem. Soc. Faraday Trans. **84**, 597 (1991).

[45]G. B. Ray and D. Leaist, J. Chem. Eng. Data **55**, 1814 (2010).

[46]A. Mialdun and V. Shevtsova, Appl. Opt. **56**, 572 (2017).

[47]A. Mialdun and V. Shevtsova, J. Chem. Phys. **138**, 161102 (2013).

[48]G. Guevara-Carrion, T. Janzen, Y. M. Munoz-Munoz, and J. Vrabec, J. Chem. Phys. **144**, 124501 (2016).

[49]T. Windmann, M. Linnemann, and J. Vrabec, J. Chem. Eng. Data **59**, 28 (2014).

[50]T. Schnabel, J. Vrabec, and H. Hasse, Fluid Phase Equilib. **233**, 134 (2005).

[51]T. Schnabel, A. Srivastava, J. Vrabec, and H. Hasse, J. Phys. Chem. B **111**, 9871 (2007).

[52]Y. M. Muñoz-Muñoz, G. Guevara-Carrion, and J. Vrabec, **Manuscript in preparation** (2018).

[53]L. Onsager, Phys. Rev. **37**, 405 (1931).

[54]S. H. Jamali, L. Wolff, T. M. Becker, A. Bardow, T. J. H. Vlugt, and O. A. Moultos, J. Chem. Theory Comput. **14**, 2667 (2018).

[55]G. M. Wilson, J. Am. Chem. Soc. **86**, 127 (1964).

[56]Dortmund Data Bank, "RecPar Software. G^E Model Parameter Regression Simultaneously to Multiple Properties," www.ddbst.com (2015).

[57]R. Taylor and H. A. Kooijman, Chem. Eng. Comm. **102**, 87 (1991).

[58]M. P. Allen and D. J. Tildesley, *Computer Simulation of Liquids* (Clarendon Press, Oxford, 1987).

[59]M. Haughney, M. Ferrario, and I. R. McDonald, J. Phys. Chem. **91**, 4934 (1987).

[60]D. G. Leaist and L. Hao, J. Phys. Chem. **98**, 4702 (1994).

[61]I. C. Yeh and G. Hummer, J. Phys. Chem. B **108**, 15873 (2004).

[62]P. W. M. Rutten, *Diffusion in Liquids* (Delft University Press, Delft, 1992).

[63]B. D. Djordjevic, I. R. Radovic, M. L. Kijevcanin, A. Z. Tasic, and S. P. Serbanovic, J. Serb. Chem. Soc. **74**, 477 (2009).

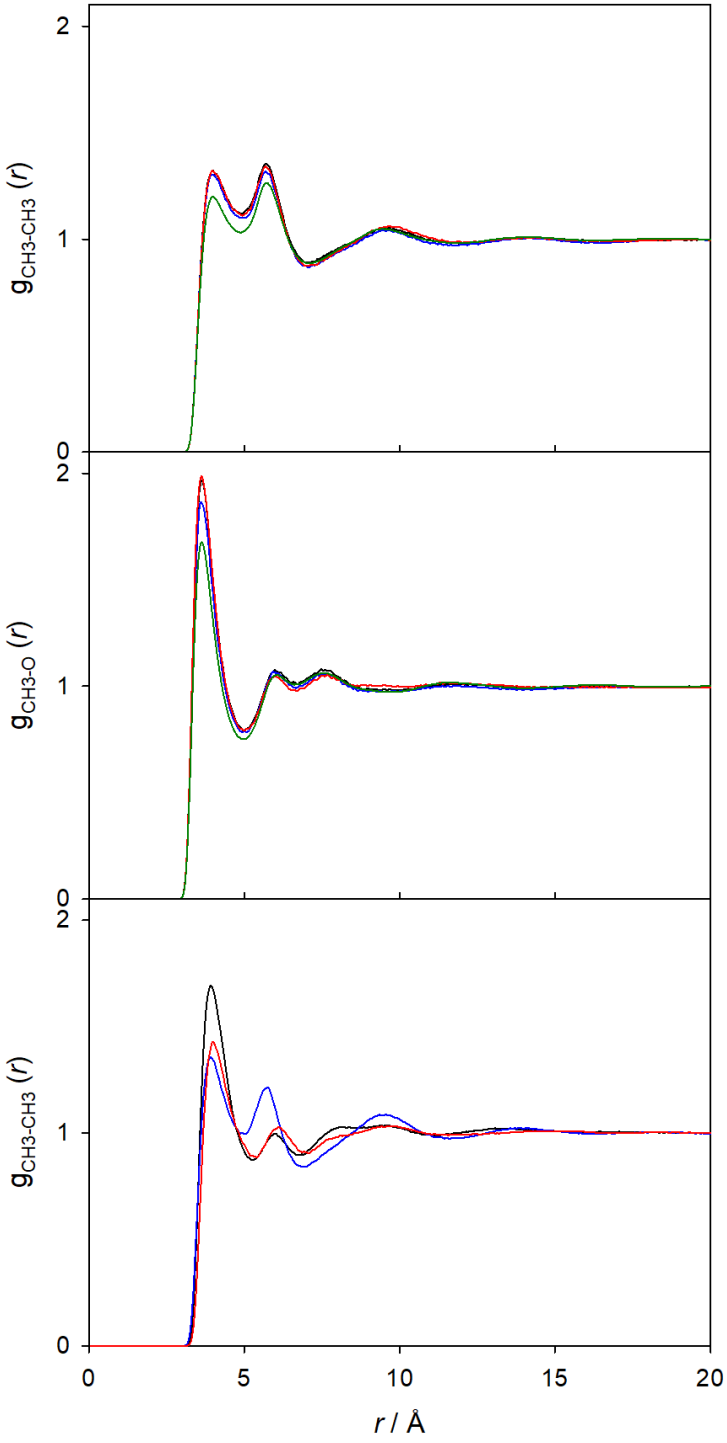

FIG. 14. Radial distribution functions of the acetone-acetone $g_{\mathrm{CH3-CH3}}(r)$ (top), $g_{\mathrm{O-CH3}}(r)$ (center) and acetone-alcohol $g_{\mathrm{CH3-CH3}}(r)$ (bottom) interactions of the equimolar ternary mixtures benzene + acetone + methanol (black) / ethanol (blue) / 2-propanol (red) at 298.15 K and 0.1 MPa. The green line represents the RDF of acetone in its pure state.

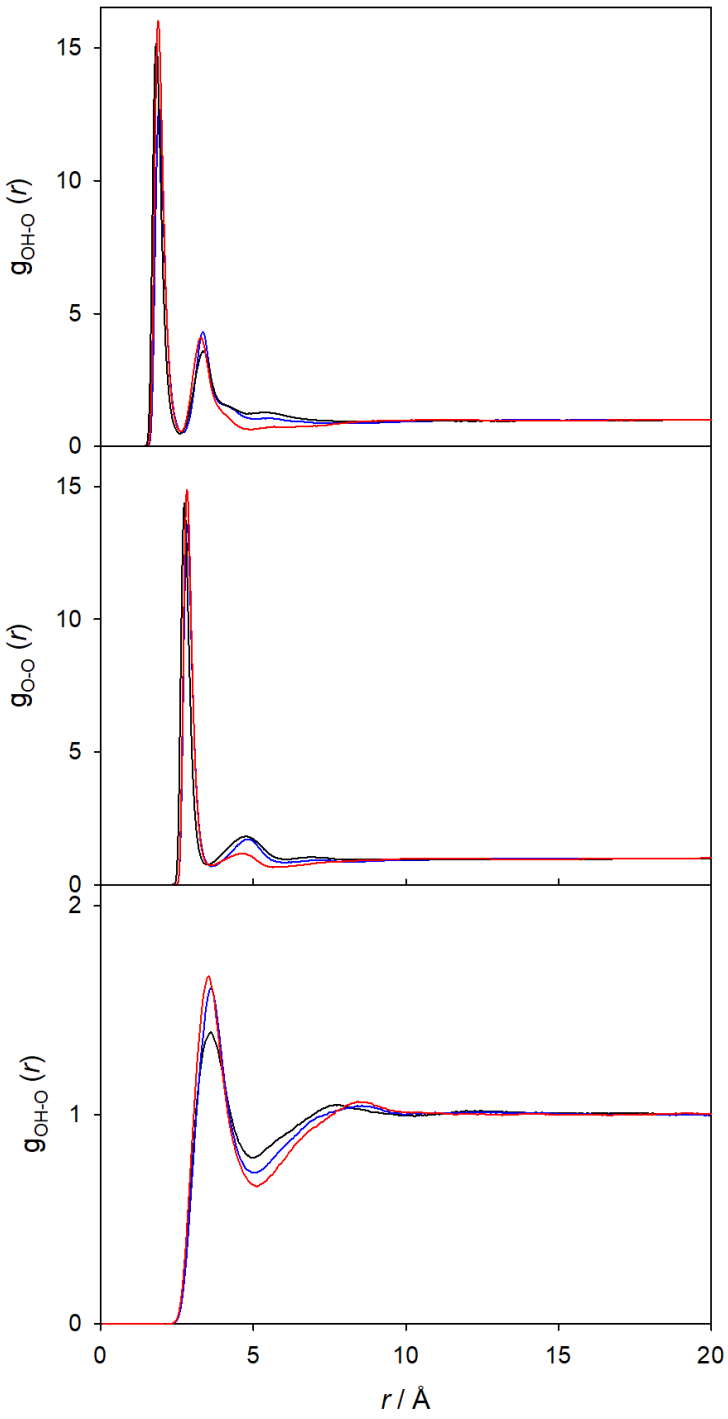

FIG. 15. Radial distribution functions of the alcohol-alcohol $g_{\mathrm{OH-O}}(r)$ (top), $g_{\mathrm{O-O}}(r)$ (center) and alcohol-acetone $g_{\mathrm{OH-O}}(r)$ (bottom) interactions of the equimolar ternary mixtures benzene + acetone + methanol (black) / ethanol (blue) / 2-propanol (red) at 298.15 K and 0.1 MPa.

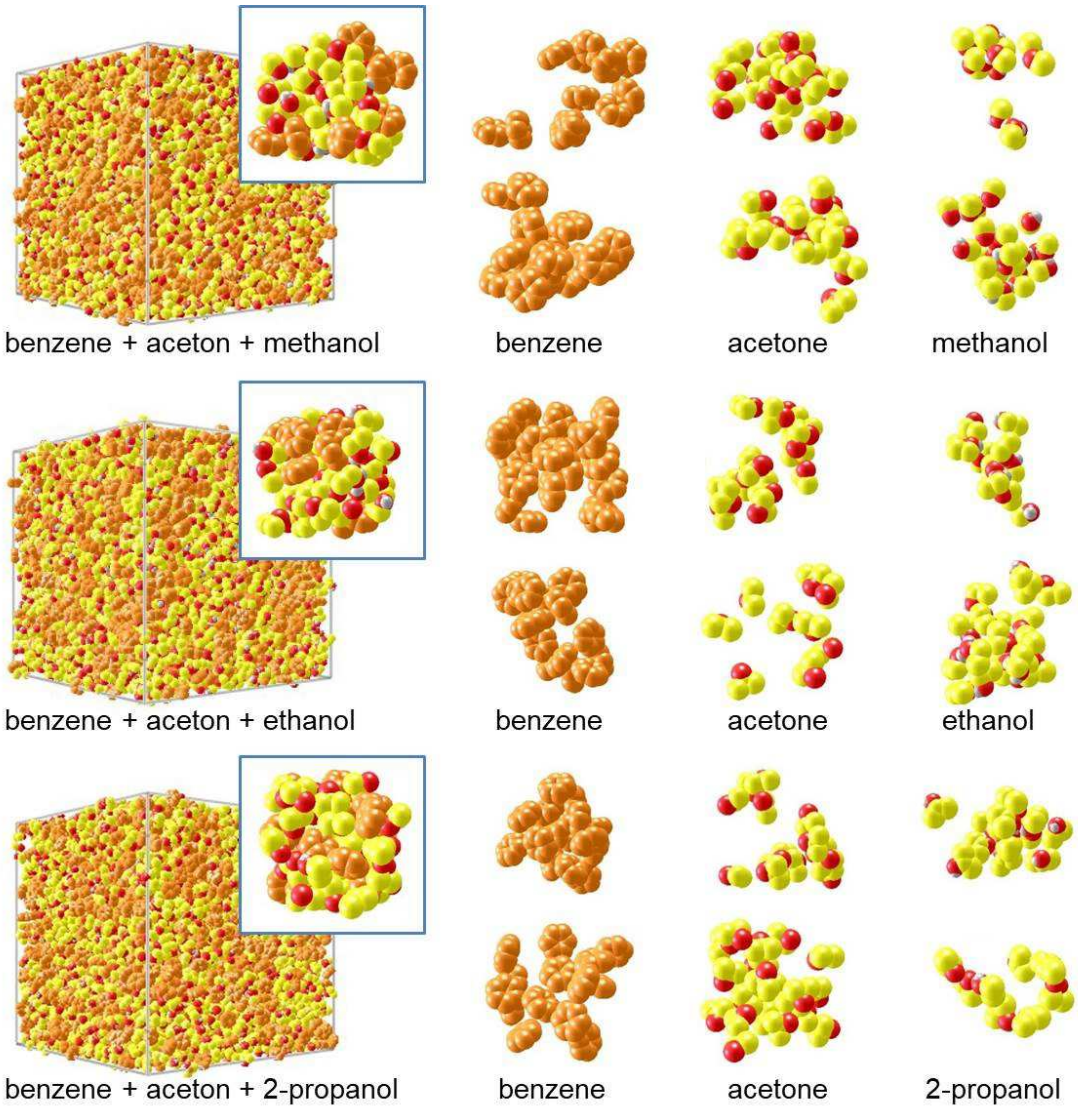

FIG. 16. Selected snapshots of the equimolar benzene + acetone + methanol (top) / ethanol (center) / 2-propanol (bottom) mixtures 298.15 K and 0.1 MPa. In the left column, all molecules are shown, whereas in the remaining columns only benzene molecules, acetone molecules or alcohol molecules are depicted. Here, the aromatic carbons are brown, oxygen molecules are red, hydroxyl hydrogens are white and methyl groups are yellow.

Supplementary Material to: Interplay of Structure and Diffusion in Ternary Liquid Mixtures of Benzene + Acetone + Varying Alcohols

Gabriela Guevara-Carrion,[1] Yuri Gaponenko,[2] Aliaksandr Mialdun,[2] Tatjana Janzen,[1] Valentina Shevtsova,[2, a)] and Jadran Vrabec[1, b)]

[1)] *Thermodynamics and Energy Technology, University of Paderborn, Warburger Str. 100, D-33098 Paderborn, Germany*

[2)] *Microgravity Research Center, Université Libre de Bruxelles, CP–165/62, Av. F.D. Roosevelt, 50, B–1050 Brussels, Belgium*

MOLECULAR SIMULATION DETAILS

Equilibrium molecular dynamics simulations were performed with the simulation tool $ms2$[1]. These were done in two steps: First, a simulation in the isobaric-isothermal (NpT) ensemble was performed to calculate the density at the desired temperature, pressure and composition. In the second step, a canonic (NVT) ensemble simulation was performed at this density to sample the transport properties. Newton's equations of motion were solved with a fifth-order Gear predictor-corrector numerical integrator. The temperature was controlled by velocity scaling. Throughout, the integration time step was 0.98 fs. Simulations were carried out in a cubic volume with periodic boundary conditions. To minimize finite size and cut-off effects, 5000 molecules were considered and the cut-off radius was set to $r_c = 17.5$ Å. The LJ long range interactions were corrected using angle averaging[2]. Electrostatic long-range corrections were considered by the reaction field technique with conducting boundary conditions ($\epsilon_{RF} = \infty$). The simulations in the NpT ensemble were equilibrated over 5×10^5 time steps, followed by a production run over 2×10^6 time steps. In the NVT ensemble, the simulations were equilibrated over 5×10^5 time steps, followed by production runs of 2×10^7 time steps with up to 1×10^5 independent time origins of the autocorrelation functions. The sampling length of the autocorrelation functions varied between 45 and 60 ps. The separation between the time origins was chosen such that all autocorrelation functions have decayed at least to 1/e of their normalized value to achieve their time independence[3]. The uncertainties of the predicted values were estimated with a block averaging method[4].

[a)] Electronic mail: vshev@ulb.ac.be

[b)] Electronic mail: jadran.vrabec@upb.de

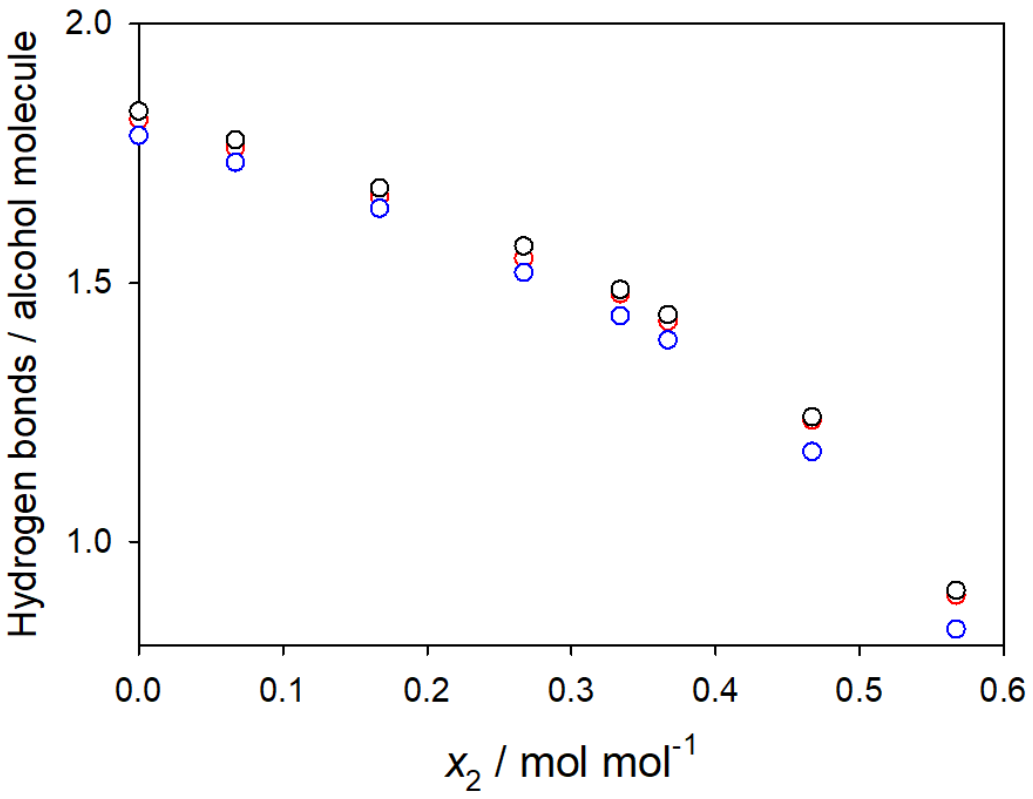

FIG. 1. Average number of hydrogen bonds per alcohol molecule of the ternary mixtures benzene + acetone + methanol (black) / ethanol (blue) / 2-propanol (red) at 298.15 K and 0.1 MPa along a constant benzene mole fraction path $x_1 = 0.33$ mol mol^{-1}. Statistical uncertainties are within symbol size.

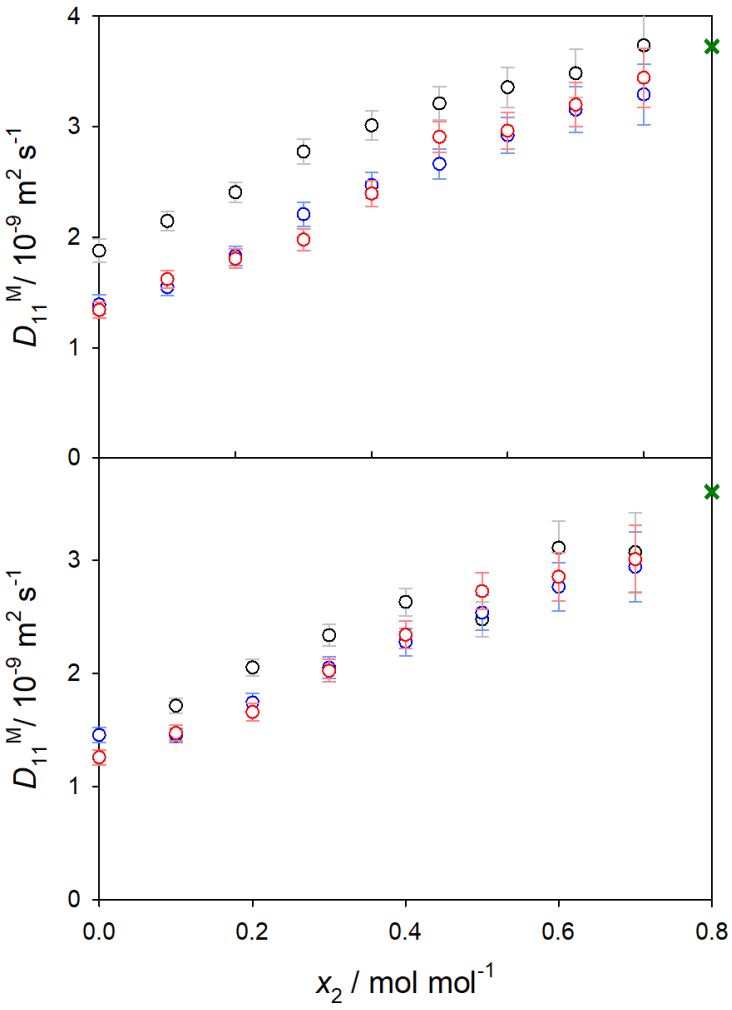

FIG. 2. Fick diffusion coefficient D_{11}^{M} matrix of the ternary mixtures benzene (1) + acetone (2) + methanol (black) / ethanol (blue) / 2-propanol (red) (3) at 298.15 K and 0.1 MPa along two constant benzene mole fraction paths x_1= 0.1 (top) and 0.2 mol mol^{-1} (bottom) from molecular simulation. The green cross indicates asymptotic values approaching the binary subsystem.

NUMMERICAL DATA

TABLE I. Parameters of the Wilson g^{E} model, where $\Lambda_{ij} = (v_j/v_i)\exp(-\Delta\lambda_{ij}/RT)$.

component 1	component 2	$\Delta\lambda_{ij}$ / J mol $^{-1}$	$\Delta\lambda_{ji}$ / J mol $^{-1}$
benzene	acetone	-378.92	1646.6
	methanol	713.71	8571.3
	ethanol	598.82	7249.1
	isopropanol	1228.5	4063.2
acetone	methanol	-602.29	2575.3
	ethanol	104.19	1630.3
	isopropanol	1096.2	969.56

component	v_i / cm^3 mol $^{-1}$
benzene	89.711
acetone	73.876
methanol	40.749
ethanol	58.372
isopropanol	77.034

TABLE II. Eigenvalues $\hat{D}_1$ and $\hat{D}_2$ in $10^{-9}\mathrm{m}^2\mathrm{s}^{-1}$ of the ternary mixtures benzene (1) + acetone (2) + methanol / ethanol / isopropanol (3) at 298.15 K and 0.1 MPa along a constant benzene mole fraction path $x_1 = 0.33$ mol mol^{-1} from present experiments and predicted by molecular simulation.

benzene + acetone + methanol						
x_1	x_2	x_3	$\hat{D}_1^{\mathrm{exp}}$	$\hat{D}_2^{\mathrm{exp}}$	$\hat{D}_1^{\mathrm{sim}}$	$\hat{D}_2^{\mathrm{sim}}$
0.33	0.07	0.60	3.23	1.42	2.87	1.32
0.33	0.17	0.17	3.34	1.61	3.27	1.52
0.33	0.27	0.25	3.68	1.82	3.46	1.75
0.33	0.33	0.37	3.73	1.99	3.77	2.03
0.33	0.37	0.44	3.74	2.05	4.00	2.15
0.33	0.47	0.50	4.17	2.34	4.50	2.66
0.33	0.57	0.60	4.50	2.57	4.87	2.95
benzene + acetone + ethanol						
x_1	x_2	x_3	$\hat{D}_1^{\mathrm{exp}}$	$\hat{D}_2^{\mathrm{exp}}$	$\hat{D}_1^{\mathrm{sim}}$	$\hat{D}_2^{\mathrm{sim}}$
0.33	0.07	0.60	2.69	1.32	2.24	1.27
0.33	0.17	0.50	2.92	1.50	2.55	1.40
0.33	0.27	0.40	3.15	1.66	2.89	1.71
0.33	0.33	0.33	3.26	1.80	3.00	1.86
0.33	0.37	0.30	3.38	1.88	3.20	1.90
0.33	0.47	0.20	3.66	2.12	3.57	2.35
0.33	0.57	0.10	3.89	2.70	3.88	2.81
benzene + acetone + 2-propanol						
x_1	x_2	x_3	$\hat{D}_1^{\mathrm{exp}}$	$\hat{D}_2^{\mathrm{exp}}$	$\hat{D}_1^{\mathrm{sim}}$	$\hat{D}_2^{\mathrm{sim}}$
0.33	0.07	0.60	2.28	1.20	2.21	1.27
0.33	0.17	0.50	2.59	1.32	2.50	1.49
0.33	0.27	0.40	2.85	1.46	2.68	1.67
0.33	0.33	0.33	3.04	1.68	2.82	1.90
0.33	0.37	0.30	3.17	1.74	3.11	1.96
0.33	0.47	0.20	3.45	2.01	3.40	2.47
0.33	0.57	0.10	3.92	2.37	3.47	2.94

TABLE III. Maxwell-Stefan diffusion coefficients $Đ_{ij}$ in $10^{-9}\mathrm{m}^2\mathrm{s}^{-1}$ and phenomenological diffusion coefficient matrix $\mathbf{\Delta}$ in $10^{-9}\mathrm{m}^2\mathrm{s}^{-1}$ together with their statistical uncertainties σ in $10^{-9}\mathrm{m}^2\mathrm{s}^{-1}$ of the ternary mixtures benzene (1) + acetone (2) + methanol / ethanol / isopropanol (3) at 298.15 K and 0.1 MPa along a constant benzene mole fraction path $x_1 = 0.33$ mol mol^{-1} predicted by molecular simulation.

benzene + acetone + methanol																
x_1	x_2	x_3	$Đ_{13}$	σ	$Đ_{12}$	σ	$Đ_{23}$	σ	Δ_{11}	σ	Δ_{12}	σ	Δ_{21}	σ	Δ_{22}	σ
0.33	0.07	0.60	5.4	0.4	1.9	0.3	4.2	0.9	4.9	0.1	1.7	0.3	0.3	0.2	3.1	0.1
0.33	0.17	0.50	6.1	0.9	2.3	0.4	5.0	1.0	5.1	0.2	1.6	0.2	0.7	0.2	3.8	0.2
0.33	0.27	0.40	6.7	1.4	2.6	0.4	5.3	1.1	5.1	0.2	1.6	0.2	1.0	0.2	4.3	0.2
0.33	0.33	0.33	7.5	1.9	2.8	0.4	5.8	1.2	5.3	0.2	1.6	0.2	1.4	0.2	4.7	0.2
0.33	0.37	0.30	7.6	2.3	2.9	0.5	6.2	1.5	5.3	0.2	1.7	0.2	1.6	0.2	5.0	0.3
0.33	0.47	0.20	9.4	4.3	3.3	0.6	5.9	1.4	5.6	0.3	1.7	0.3	1.7	0.2	5.2	0.3
0.33	0.57	0.10	10.2	6.4	3.5	0.6	5.3	1.2	5.3	0.3	1.5	0.3	1.3	0.2	4.8	0.3
benzene + acetone + ethanol																
x_1	x_2	x_3	$Đ_{13}$	σ	$Đ_{12}$	σ	$Đ_{23}$	σ	Δ_{11}	σ	Δ_{12}	σ	Δ_{21}	σ	Δ_{22}	σ
0.33	0.07	0.60	3.4	0.2	1.8	0.3	2.8	0.5	3.3	0.1	0.7	0.3	0.1	0.2	2.4	0.1
0.33	0.17	0.50	4.0	0.4	2.3	0.3	3.0	0.4	3.6	0.1	0.6	0.2	0.2	0.2	2.7	0.1
0.33	0.27	0.40	4.8	0.8	2.4	0.3	4.0	0.7	3.9	0.1	0.9	0.2	0.6	0.2	3.4	0.2
0.33	0.33	0.33	5.2	0.9	2.6	0.4	4.0	0.6	4.1	0.2	0.9	0.2	0.6	0.2	3.5	0.2
0.33	0.37	0.30	4.9	0.8	2.9	0.4	4.1	0.6	4.0	0.2	0.7	0.2	0.5	0.2	3.7	0.2
0.33	0.47	0.20	5.6	1.3	3.2	0.5	4.4	0.6	4.3	0.2	0.7	0.2	0.7	0.2	4.0	0.2
0.33	0.57	0.10	5.3	1.4	3.7	0.5	4.1	0.5	4.4	0.2	0.5	0.2	0.2	0.1	4.0	0.3
benzene + acetone + 2-propanol																
x_1	x_2	x_3	$Đ_{13}$	σ	$Đ_{12}$	σ	$Đ_{23}$	σ	Δ_{11}	σ	Δ_{12}	σ	Δ_{21}	σ	Δ_{22}	σ
0.33	0.07	0.60	3.1	0.2	1.9	0.4	2.6	0.4	3.0	0.1	0.4	0.2	0.1	0.1	2.3	0.1
0.33	0.17	0.17	3.6	0.3	2.3	0.4	3.1	0.4	3.4	0.1	0.5	0.2	0.2	0.2	2.8	0.1
0.33	0.27	0.25	3.9	0.5	2.6	0.4	3.5	0.4	3.5	0.1	0.5	0.2	0.3	0.2	3.2	0.1
0.33	0.33	0.37	4.4	0.6	2.9	0.4	4.0	0.4	3.8	0.2	0.5	0.2	0.2	0.2	3.3	0.2
0.33	0.37	0.44	4.0	0.5	3.2	0.4	4.5	0.5	3.7	0.2	0.3	0.2	0.3	0.2	3.7	0.2
0.33	0.47	0.50	4.6	0.8	3.3	0.5	3.7	0.6	3.9	0.2	0.4	0.2	0.6	0.1	4.1	0.2
0.33	0.57	0.60	5.4	1.4	3.7	0.5	3.0	0.4	4.3	0.2	0.5	0.2	0.4	0.1	3.7	0.3

BIBLIOGRAPHY

[1]C. W. Glass, S. Reiser, G. Rutkai, S. Deublein, A. Köster, G. Guevara-Carrion, A. Wafai, M. Horsch, M. Bernreuther, T. Windmann, H. Hasse, and J. Vrabec, Comp. Phys. Commun. **185**, 3302 (2014).
[2]R. Lustig, Mol. Phys. **65**, 175 (1988).
[3]M. Schoen and C. Hoheisel, Mol. Phys. **52**, 33 (1984).
[4]M. P. Allen and D. J. Tildesley, *Computer Simulation of Liquids* (Clarendon Press, Oxford, 1987).